AMORPHOUS SILICON SOLAR CELLS

B.W. CLARE, J.C.L. CORNISH, G.T. HEFTER, P.J. JENNINGS, C.P. LUND,
S.R. PHILLIPS, G.N. RAIKAR and G.P. THAMBIRASA

School of Mathematical and Physical Sciences
Murdoch University, Murdoch, WA 6150, Australia

S.H. CHEAH and J. LIVINGSTONE

Department of Electrical Engineering
University of Western Australia, WA 6009, Australia

C. KLAUBER

CSIRO Division of Minerals and Geochemistry
Bentley, WA 6102, Australia

Research Report : May 1987

ABSTRACT

Thin films of hydrogenated amorphous silicon have been prepared by chemical vapour deposition at atmospheric pressure from a mixture of silanes over a heated substrate. This approach provides an alternative method to glow discharge and it has several substantial advantages, including safety and lower costs. High deposition rates have been obtained by use of a silent electrical discharge in the gas stream prior to the deposition process.

Solar cells fabricated from these films show open circuit voltages of up to 400 mV but current densities are low. This is attributed to a low hydrogen content in the films. Physical and chemical characterization techniques have been used to identify the limiting factors in the performance of these devices. Further research is proposed to improve the efficiency of the photovoltaic devices.

1. INTRODUCTION

Amorphous silicon (a-Si) is one of the most promising new materials for the production of thin film photovoltaic (PV) cells. Although this material is relatively new it has already reached a stage of development where it is being used in commercial PV devices. However, there are still a considerable number of problems with amorphous silicon which must be overcome if solar cells of this material are to capture a large slice of the PV market. Many of these problems arise from our inadequate understanding of the nature and properties of amorphous materials. Most of the recent advances in amorphous silicon technology have come about through technological research, which aims to produce better devices. There is still a lack of fundamental knowledge about the structure and bonding in amorphous silicon and the role which these play in determining its photovoltaic properties.

1.1. Review

The current interest in amorphous silicon began with the work of Chittick et al in 1969 [1]. At that time many people believed that a-Si would not show any PV properties. However, in 1977 Spear [2] and others demonstrated that PV quality amorphous silicon films could be produced by using a radiofrequency glow discharge in silane ($Si\ H_4$). Soon after a number of workers [3] showed that PV quality amorphous silicon required at least 10% of hydrogen in its lattice. The hydrogen apparently reduces the density of dangling bonds present in elemental amorphous silicon lattices and produces a material which is suitable for semiconductor devices such as solar cells. Other researchers [4] have claimed that the incorporation of fluorine into the a-Si:H alloy produces a further reduction in the dangling bond density and also improves the stability of the material with respect to photodegradation. This is an active area of research as photodegradation of amorphous silicon is one of the major technological problems which limits its value as a photovoltaic material. At the present time some researchers have achieved efficiencies of over 10% for *pin* junction solar cells based on amorphous silicon [5] while ECD claim an efficiency of 13% for their tandem fluorinated cells.

Although the best reported efficiencies for amorphous silicon are well below those for single crystal and polycrystalline silicon solar cells, all three technologies are able to produce modules of comparable price (~US$5 per peak watt in 1986). This is because amorphous silicon panels can be fabricated from the cells at a lower cost than those based on crystalline or polycrystalline silicon. The reasons for this are :

(1) Amorphous silicon has a much larger absorption coefficient and so only very thin layers (<1 μm thick) are required.

(2) Amorphous silicon can be grown inexpensively by a chemical process using a readily available gas ($Si\ H_4$), while crystalline silicon involves costly procedures of crystal growth and cutting.

(3) The raw materials required for amorphous silicon production do not need to be as pure as those used in crystalline silicon work because the former are easily purified in the gas phase. Also, amorphous materials may be inherently more tolerant of impurities than single or poly-crystalline materials.

(4) Amorphous silicon films may be deposited on inexpensive substrates such as stainless steel or glass.

Also, the use of thin film technology has enabled producers to make *pin* and tandem or multiple junction devices in-situ. Thus a tandem device can use very thin films and it can be engineered so that each of the two cells is made from material with a different band gap. This increases the efficiency of utilisation of solar radiation.

Another advantage of amorphous silicon is that it lends itself to large-scale industrial production. Because it is a thin film material it can be deposited on a continuous roll of plastic or stainless steel or on large sheets of glass. Thus as the market size increases, amorphous silicon technology is well-adapted to provide significant economies of scale.

1.2. Methods Used to Prepare Amorphous Silicon

There are three main deposition methods in use :

(a) Radiofrequency glow discharge is currently the principal method used to produce a-Si-H solar cells. It uses radiofrequency radiation to dissociate silane gas over a heated substrate (at about 250°C) to produce thin films of amorphous silicon. Doping is achieved by use of B_2H_6 or PH_3 in the gas stream. Some researchers use $Si F_4$ also to produce fluorinated material. This approach yields good results but it is hazardous because it requires the storage of large quantities of toxic and flammable gases. It also requires low pressures and hence the thin films must be fabricated in a vacuum system.

(b) Radiofrequency sputtering from a hot silicon target in an atmosphere of hydrogen and argon can produce films with photovoltaic properties. However, the technique is slow and expensive and does not lend itself readily to industrial production of large area solar cells.

(c) Chemical vapour deposition (CVD) involves the deposition of a-Si:H from a stream of gases passed over a hot substrate. There are many variations of this process in use, some use ultraviolet light or mercury vapour to catalyse the deposition process. Atmospheric pressure CVD uses the higher silanes (Si_2H_6, Si_3H_8 etc.) which decompose readily at around 400°C to produce thin films of hydrogenated amorphous silicon. An advantage of this approach is that it does not require large quantities of bottled gases as all of the required reactants can be produced in small quantities immediately prior to use. This has considerable advantages in cost and safety although it is more difficult to maintain quality control.

1.3. The Ellis-Gordon Approach to Amorphous Silicon

Recently Ellis and Gordon [6] have published a simple atmospheric pressure CVD method for producing good quality a-Si:H. This approach offers several advantages over the glow discharge method :

(1) It gives high growth rates for the a-Si:H films.

(2) It does not involve the use of bottled gases.

(3) It does not require the use of expensive vacuum chambers and pumps.

Like the other thin film methods, it lends itself readily to large-scale continuous roll production of a-Si:H. This technique is relatively new and it has not yet been researched to the same extent as the glow discharge method. It is therefore still uncertain whether it is capable of producing material of sufficient quality to supplant the glow discharge approach. However, in view of its considerable advantages and great promise, we decided to investigate its application. Our aim is to reproduce the Ellis-Gordon experiment and then attempt to optimize the performance of the films produced. This involves a careful physical and chemical study of their properties and characteristics to determine what factors limit their performance.

In the Ellis-Gordon approach, magnesium silicide is added to dilute acid at room temperature (HCl, H_3PO_4 or HF) to produce silane, hydrogen and the higher polysilanes

$$n\ Mg_2\ Si + 4n\ H^+ \rightarrow Si_n\ H_{2n+2} + 2n\ Mg^{++} + (n - 1)\ H_2$$

Helium or hydrogen is used as the carrier gas to transport the gas mixture through the apparatus (see Fig. 1.1). A drying column filled with molecular sieves is used to remove water vapour. Phosphorus doping is achieved by passing the gas stream through a column of phosphorus pentoxide. This produces phosphine (PH_3) via the reaction

$$5\ Si\ H_4 + 2\ P_2\ O_5 \rightarrow 4\ PH_3 = 5\ Si\ O_2 + 4H_2$$

The substrates for the a-Si:H thin films rest on a hot plate in a deposition chamber and are heated from below to a temperature of approximately 430°C.

Ellis and Gordon conclude that there are three key conditions for high deposition rates and acceptable hydrogen content in the films. These are :

(1) Higher polysilanes are essential in the gas stream.

(2) A small vertical temperature gradient decreasing away from the substrates to reduce the nucleation of crystallites.

(3) An optimized flow rate and temperature in the reactor chamber.

In the reaction chamber the higher silanes undergo thermal decomposition to produce silylene radials

$$Si_2\ H_6 \rightarrow Si\ H_2 + Si\ H_4$$

$$Si_3\ H_8 \rightarrow Si\ H_2 + Si_2\ H_6$$

etc.

The amorphous silicon lattice is thought to grow via the addition of silylene radials to Si-H bonds at the surface of the film. The silane $Si\ H_4$ plays no role in the reaction and it passes through the deposition chamber and is removed by the scrubbers, which contain dilute Na OH.

The amorphous silicon produced by this process is thought to be tetrahedrally-coordinated but with no long range order in the lattice. It includes regions of microcrystallinity and microvoids associated with dangling bonds, some of which are passivated by hydrogen atoms, as shown in Fig. 1.2.

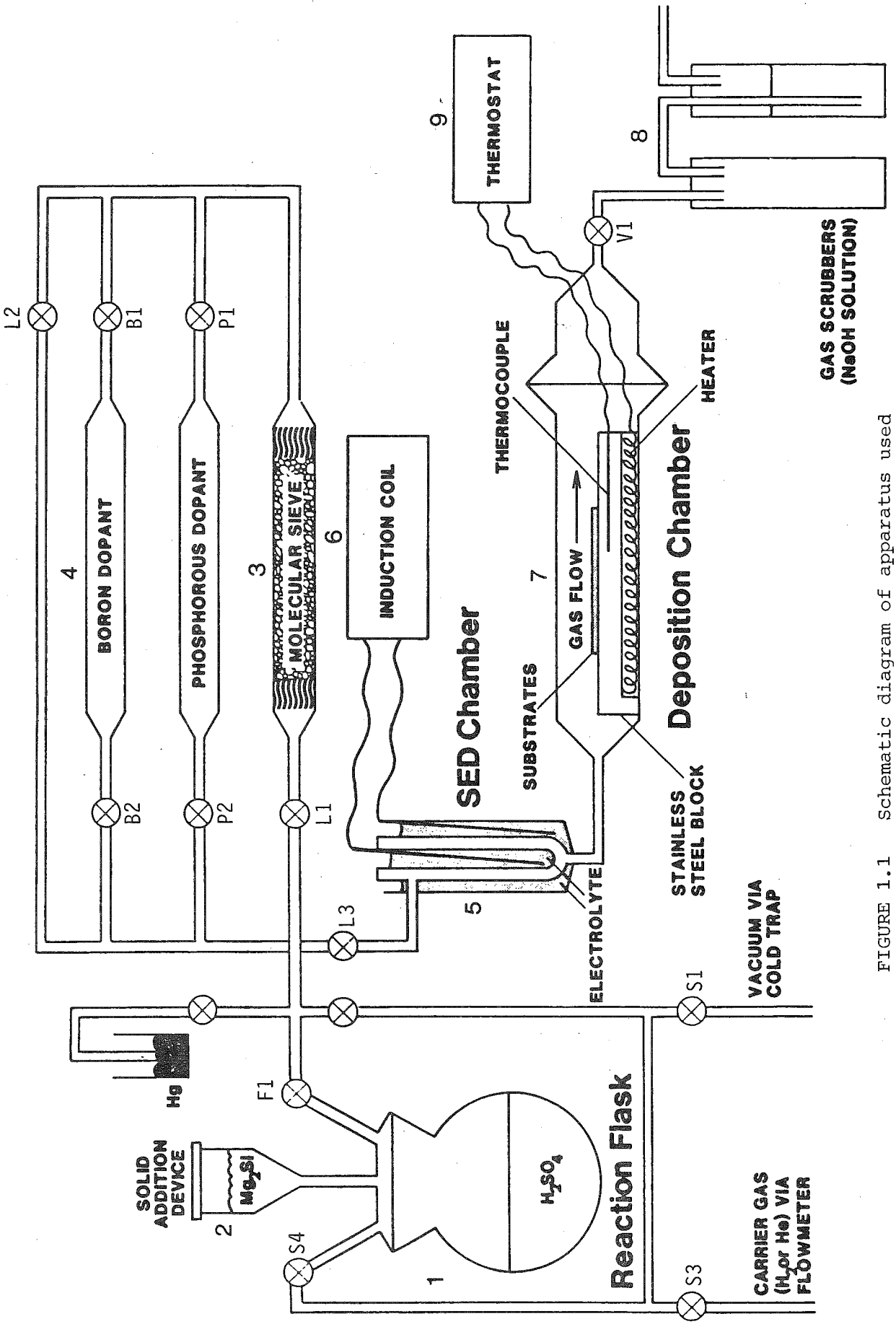

FIGURE 1.1 Schematic diagram of apparatus used in this study for atmospheric pressure CVD.

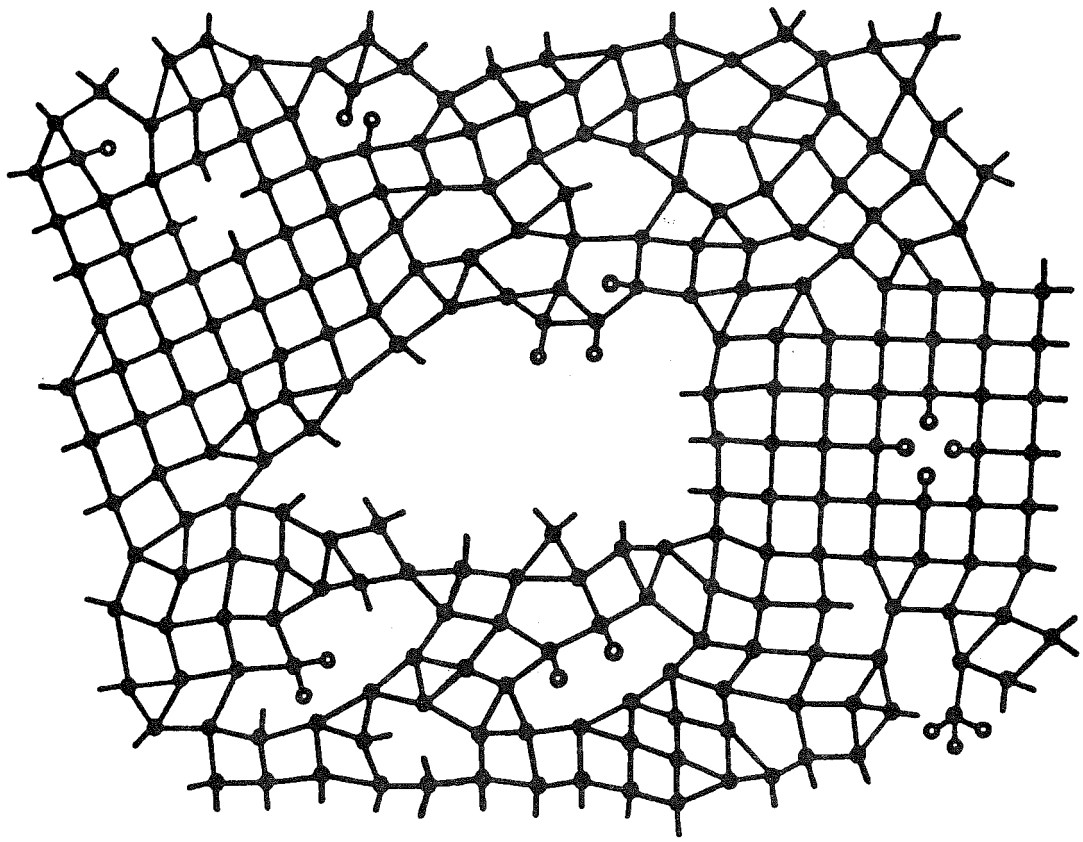

FIGURE 1.2 Two dimensional representation of a random a-Si:H network showing two regions of micro-crystallinity, a large void, dangling bonds, in mono, di and trihydride configurations.

2. FILM PREPARATION

Hydrogenated amorphous silicon (a-Si:H) films are prepared by the method developed by Ellis and Gordon [6], which was described in Section 1.3. Their procedure involves production of a gaseous mixture of hydrogen and silanes by the reaction of powdered magnesium silicide with dilute acid in a chemical reaction vessel.

$$n\ Mg_2\ Si(s) + 4n\ H^+\ (aq) \rightarrow 2n\ Mg^{2+}(aq) + (n - 1)\ H_2(g) + Si_n\ H_{2n+2}(g)$$

The silane mixture is swept from the reaction vessel with high purity He or H_2, dried, and then passed into a heated tube where the silanes pyrolize to produce specular films of a-Si:H. The general features of the apparatus are shown schematically in Fig. 1.1.

2.1. Modifications to Ellis and Gordon's Procedure

Although Ellis and Gordon's procedure was initially followed closely, a number of significant modifications have been introduced :

(a) Preparation of silanes

Hydrochloric acid which was advocated by Ellis and Gordon, for use in the reaction vessel, was discarded in favour of the less voltatile sulphuric acid. This minimized contamination of the gas stream by acid vapour and also prevented clogging of the solid addition device by premature reaction of the acid vapour with the Mg_2 Si in the device itself. It is interesting to note that in more recent reports Gordon and co-workers [7] have been using an even more volatile HCl/HF mixture. For practical purposes the acid concentration was higher and the reaction flask smaller than those used by Ellis and Gordon.

(b) Solid addition device

A solid addition device for the controlled delivery of powdered Mg_2 Si to the reaction vessel was developed (see Fig. 1.1). The device is constructed from stainless steel and consists of a conical hopper, emptied by an Archimedean screw driven by a compact, geared electric motor. The whole device is wrapped with a heating tape and kept at a higher temperature (ca. 100°C) than the reaction vessel to avoid condensation.

A significantly-improved solid addition device has now been developed and is currently being tested. Its features include greater ease of evacuation, more controlled delivery rates, less tendency to clog and better temperature control.

(c) Carrier gas

Experiments indicated little difference in film quality when helium, employed by Ellis and Gordon, was replaced by the cheaper hydrogen. However, the use of a silent electrical discharge to enrich the gas stream necessitated a return to He because hydrogen atoms react with the free radicals produced in this process.

(d) Ellis and Gordon have made detailed studies of a variety of experimental parameters in an attempt to optimize film growth [8]. One of the most important variables was found to be the concentration of higher silanes ($n > 2$) in the gas stream, since they decompose at lower temperatures than the lower silanes and they give films with a higher hydrogen content. Both these factors are believed to be conducive to better electrical characteristics in the resulting films. Unfortunately, the concentrations of higher silanes produced in the Mg_2Si/H^+ reaction are low, typically constituting less than 10% of the total gas stream [5].

One of the standard laboratory procedures for producing higher silanes is to subject the lower silanes to a silent electrical discharge (SED) in a manner similar to the production of ozone from air [9]. Thus a SED chamber was incorporated into the line (Fig.1.1) to enhance the concentration of higher silanes in the gas stream.

The production of higher silanes during a SED is believed to involve the creation of reactive silylene radicals

$$Si\ H_4 \xrightarrow{SED} Si\ H_2: + 2H$$

followed by recombination

$$Si\ H_4 + Si\ H_2: \rightarrow Si_2\ H_6 \text{ etc.}$$

Since molecular (or atomic) hydrogen is likely to scavenge the $Si\ H_2$: radicals

$$Si\ H_2: + H_2 \text{ (or } H\bullet) \rightarrow Si\ H_4$$

This inhibits higher silane production and therefore H_2 was replaced by He as the carrier gas. The enhanced deposition rates in the presence of He were confirmed by experiment.

Other researchers have used mercury vapour and ultraviolet irradiation of the gas stream to achieve the same effect [10]. We have also begun to experiment with this technique.

(e) Chemical vapour deposition vessel

Ellis and Gordon used a CVD vessel of rectangular cross-section with an external hot plate, purportedly to ensure a vertical temperature gradient and prevent particles nucleating in the gas phase and thus settling on the substrates. In our experiments this arrangement led to difficulties in the control of substrate temperature. Furthermore, Baron et al [11] have reported successful a-Si:H film growth in a cylindrically-heated tubular vessel. Consequently, a tubular pyrex vessel containing a hemi-cylindrical stainless steel block has been adopted. Controlled heating is provided by a W cartridge heater and thermocouple embedded in the block. The leads to these are taken through a pyrex cap with tungsten-to-glass seals. This arrangement has provided better temperature control and has not led to any problems from gas phase nucleation.

2.2. Apparatus and Procedure

2.2.1. Apparatus

The apparatus in Fig. 1.1 is based on a dual manifold gas/vacuum line. Vacuum is provided, via a cold trap, by a two-stage rotary pump. The gas manifold is connected at one end through a flowmeter to cylinders of hydrogen and helium, and at the other to a mercury trap, which allows a positive pressure of 2-3 mm Hg or a negative pressure of 50 mm Hg. Teflon-in-glass, vacuum stopcocks are connected across the two tubes, terminating in standard glass tapers so that each taper can be opened to either vacuum or gas.

Silane is generated in a 1 litre flangetop flask, fitted with a top containing five B19 sockets. One of these sockets is connected by rubber vacuum hose to one of the cones on the line (Stopcocks S2 and S4). Another is connected through a vacuum stopcock (F1) to a T-piece, another arm of which is connected to another of the cones on the line (Stopcocks S1 and S3), and the third to a two-way vacuum stopcock (L1). From here, a tube leads to a column containing molecular sieves, which is wound with a high temperature electrothermal tape. The column is connected to a set of three tubes, connected in parallel. One of these is 8 mm glass, with a single vacuum stopcock (L2). The other two have a vacuum stopcock at each end and between these, a 22 mm diameter section which is removable, having an O-ring seal at each end. These removable tubes can contain boron and phosphorus dopants respectively. The stopcocks at the ends of them will be designated B1 and B2, and P1 and P2 respectively. The exit from these three parallel tubes leads to a second three-way vacuum stopcock (L3), and from here, to the SED vessel and through an O-ring seal, to the CVD vessel. Gaseous effluent from the CVD vessel is taken through a vacuum stopcock V1 by vinyl tubing to a trap, which allows the gas to bubble through sodium hydroxide solution but does not allow liquid to enter the line in the event of accidental evacuation. The dopant tubes are wound with low-temperature electrothermal tapes.

The central socket on the flangetop flask bears the solid addition device, described earlier. An engraving tool, driven through a simmerstat, makes contact with the hopper and serves as a vibrator to prevent sticking of the magnesium silicide. The top of the hopper is connected by rubber pressure tubing to a socket on the flask. A thermometer occupies the fifth socket of the flask.

In a recent modification, the hose from S2 leads to a T-piece bearing two vacuum stopcocks. This allows the silane, continuously generated in the flask, to be diverted to waste, giving closer control over deposition. Thus the growth of a layer can be rapidly terminated, and the CVD chamber evacuated, in preparation for the deposition of a layer of a different type. One of these tubes terminates in the socket in the flask, the other leads through vinyl tubing and a T-piece to the bubbler.

2.2.2. Procedure

Before each run, the CVD tube and block are immersed in hot 20% sodium hydroxide, to remove silicon deposits from the previous experiment. The block is polished with abrasive paper and immersed in chromic acid cleaning mixture to remove grease. Both are then treated in an ultrasonic bath with

Decon 90 solution followed by ultrapure water, then dried. A solution of 60 ml concentrated sulphuric acid in 200 ml water is placed in the flask and a mixture of magnesium silicide, with silica as diluent, is placed in the solid addition device. After the CVD vessel is cleaned, loaded with the substrates in a laminar flow clean cabinet, and placed in position on the line, hydrogen is passed through the gas tube and the vacuum side is evacuated. Stopcock S1 is opened, F1 is closed, and L1, L2, L3 are opened, and V1 is closed. Thus the line is evacuated and the gas side flushed. Stopcock S1 is closed and S3 carefully opened (avoiding any suckback in the mercury bubbler). Stopcock V1 is opened, allowing hydrogen to escape through the sodium hydroxide trap. After flushing for 15 minutes, stopcocks V1 and S3 are closed and S1 opened. This evacuates the vessel again and when the pressure is lowered to 1 mm Hg, S1 is closed and S3 carefully opened. When the pressure reaches atmospheric, V1 is opened, allowing the gas to escape through the caustic. The heater in the block is then turned on, with the thermostat set to 120°C. After 30 minutes at this temperature the thermostat is turned to 450°C and stopcocks L1 and S3 closed. Hydrogen should continue to bubble very slowly through the caustic, as the hydrogen in the CVD vessel expands. With liquid nitrogen in the cold trap, stopcocks S1 and F1 are opened, evacuating the reaction flask. When the pressure stabilises, usually at 0.3-0.5 mm Hg, S1 is turned off and S3 carefully opened. When the pressure in the flask has reached atmospheric, L1 is opened and hydrogen is allowed to flush through the CVD vessel until the temperature reaches 450°C. After 15 minutes at this temperature the thermostat is turned to the desired temperature (typically 430°C) and the hydrogen is turned off and the helium on. The induction coil on the SED apparatus is now turned on, and after 5 minutes, the solid addition device and the vibrator are turned on. Timing begins from when magnesium silicide first drops into the acid.

A run is normally continued for 30 minutes after the magnesium silicide runs out, that is usually a total time of about 90 minutes. On completion of the run, helium is turned off, hydrogen on, the heater off, stopcocks F1 and S4 off and S3 on, isolating the silane generator and passing hydrogen through the CVD vessel while it cools. The vessel is allowed to cool under hydrogen for at least an hour before being opened and the substrates removed.

2.3. Experimental Conditions

2.3.1. Silane generation

The conditions used vary from those of Ellis and Gordon in that the acid used was sulphuric, at somewhat higher concentration, and the reaction began at ambient temperature. In the early stages, a charge of 7 g magnesium silicide and 7 g silica as diluent was used, but this resulted in too thin a film at the deposition conditions then being used. Later, 40 g of this mixture was used, with a solution of 60 mL of sulphuric acid in 200 mL water. With these conditions, and the solid addition device on 3/8 speed, the temperature of the flask rose from ambient to 80-90°C over the hour taken to complete the addition. These quantities resulted in

films approximately 3 μm thick, under the typical deposition conditions. Thinner films obviously can be grown with smaller charges, shorter deposition times and lower deposition temperatures.

2.3.2. Deposition conditions

In the earliest experiments, using a rectangular CVD tube, the hotplate was run at 600°C and film thicknesses of the order of 0.2 μm were attained. With the introduction of the SED vessel and the use of the larger charge of silicide, films 3 μm or more in thickness were obtained. Films of thickness greater than 2 μm have a tendency to peel. The block temperature most frequently used in recent experiments was 430°C. Note, however, that this is the temperature experienced by the thermocouple. The actual temperature of the block, and especially the temperature of the substrates, may vary from this figure by up to 50°C.

2.4. Optimisation of Conditions

With the rectangular CVD tube on the plate at 600°C, a set of fringes was obtained in 8 minutes. A flow rate of 800 mL/min. was used. Little optimisation of temperature could be achieved with the rectangular vessel as the operating temperature (600°C) was the maximum which could be attained with this setup, and clearly, a higher temperature was needed. The deposition rate was also very variable, owing to the poor (and nonreproducible) contact between the block and vessel. With helium in the rectangular tube, deposition periods ranged from 1 to 20 minutes per set of fringes, at temperatures of 590 to 615°C, with little correlation with temperature. No optimisation with hydrogen was attempted with the rectangular vessel.

With the cylindrical tube and internal block, a much better control was achieved. With a helium flow rate of 800 mL/min and a block temperature of 420°C, a period of 4 minutes per set of fringes was obtained. With hydrogen as carrier, a block temperature of 420°C and a flow rate of 600 mL/min, a deposition period of approximately 7 minutes per set of fringes was observed. At the lower temperature of 390°C this increased to 20-30 minutes.

Under typical conditions, a specular film of a-Si:H is deposited on the blank substrates and (eventually) the vessel walls. The deposition zone is about 10 cm in length and thins out towards either end. The film thickness remained reasonably constant within a distance of 3-4 cm from the centre of location of the substrates (which approximates to the reaction zone centre). No radial thickness variation has been apparent. Up to six substrates (of dimensions 2 cm × 1 cm) can be coated per run, with a variation of film thickness of <10% (i.e. ca. 0.2 μm). Films are generally specular although occasionally powdery or opalescent films are obtained. These are discussed in Section 4.1.

The enrichment of the gas stream by the use of a silent electrical discharge has led to a marked improvement in the rate of deposition. The earliest experiments involved holding the probe of a spark tester (Tesla coil) near the CVD vessel, causing a discharge to the block. Hydrogen was used as carrier gas in these experiments. This led to an increase of about 50% in deposition rate and was followed up by the construction of a vessel of a design based on an ozoniser. With 24 kilovolts applied to this from a laser power supply, no perceptible effect was obtained. When the output of a lecture demonstration-type

induction coil was applied to this vessel, however, the period decreased from 30 minutes per fringe set to about 10 minutes.

Based on the reasoning that atomic hydrogen would interfere with the production of higher silanes by scavenging free radicals (see Section 2.1 (c)), the effect of using helium as carrier was investigated. This resulted in a very noticeable increase in the deposition of a yellow byproduct (thought to be silicon subhydrides [9]) in the CVD tube and a reduction of the temperature threshold for deposition from 390 to 365°C. At 430°C the period between successive fringes was about 2 minutes and at 450°C, about 1 minute. These times are rather variable but are much more consistent than those involving the flat tube.

2.5. Doping with Phosphorus and Boron

Two vessels were built into the line for introducing dopants into the gas stream (Fig. 1.1). These were arranged so that the silane in the carrier gas could be diverted through them with appropriate stopcocks. One of these tubes contained phosphorus pentoxide, the other contained decaborane-14. Both tubes were wrapped with low temperature electrothermal heating tapes.

Phosphorus doping was accomplished by using the apparatus in the usual way except that the gas stream was passed through the phosphorus pentoxide tube by closing stopcock L2 and opening P1 and P2. Phosphine is produced by the reaction between phosphorus pentoxide and silane, as outlined in Section 1.2.

The temperature of the phosphorus pentoxide tube was maintained at 60-100°C. At the higher end of this range deposition of silicon was slowed by about 50%, otherwise, no difference was observed to a normal intrinsic run. A SED was used, as described above for deposition of intrinsic material.

Boron doping was achieved by passing the silane in a helium stream over warmed decaborane, via the second doping tube (that is, by opening stopcocks B1 and B2 and closing L2, P1 and P2). The decaborane was held at ~40°C. At this temperature, rapid depositon of amorphous silicon occurred, with a block temperature of 380°C. The period was about 3 minutes per set of fringes under these conditions (a five-fold enhancement of the deposition rate). A noticeable characteristic of the silicon deposited under these conditions was its extreme chemical inertness. It was not attacked by hot, concentrated alkali, by acids, including hydrofluoric, or by high temperatures in air.

Some unsuccessful attempts were made to produce *pin* devices. An n-type film was deposited by running the apparatus as described for phosphorus doping, until two sets of fringes had appeared. The silane stream was then diverted to the caustic trap while the gas in the line, including the CVD vessel, was flash pumped. The phosphorus tube was then closed off, helium was re-admitted to the line and the silane was directed once more through the CVD vessel. An intrinsic layer was deposited for 30 minutes and then the temperature of the block was dropped to 380°C. The silane stream was diverted through the decaborane and the P layer was deposited for about 5 minutes. The devices obtained were unsuccessful, probably due to extensive contamination of the line with decaborane. It proved necessary to thoroughly clean the line (partly by heating, partly by wet chemical methods) to remove this contamination.

3. SUBSTRATE PREPARATION

3.1. Choice of Substrate

One of the advantages of amorphous silicon is that it can be deposited on a variety of low-cost substrates. Amongst the most popular choices are glass or plastic, coated with a transparent conducting oxide such as indium tin oxide. Stainless steel is also widely used as a substrate for amorphous silicon because of its stability and low cost.

We decided to use stainless steel for these experiments because of its ready availability and ease of preparation. There are several different types of stainless steel available, each with a somewhat different composition, which could affect the properties of the a-Si:H films deposited on them. For this reason it is customary to passivate the stainless steel surfaces before the silicon films are deposited. The passivation also prevents the formation of a Schottky barrier at the substrate-semiconductor junction. Ideally the passivation should produce a thin oxide film which improves the adhesion of the a-Si:H film and prevents undesirable reactions between the semiconductor and the substrate. The oxide film should be sufficiently thin so that it does not significantly increase the series resistance of the photovoltaic device.

3.2. Stainless Steel Substrates

3.2.1. Stainless steel substrate preparation

The preparation procedure for stainless steel was developed over an eighteen month period by Stephen Phillips. The quality of the deposited film was found to be critically dependent upon the meticulous application of this technique.

Stainless steel in sheet form, 0.5 mm thick, was cut into 10 × 20 mm rectangular pieces, keeping them as flat as possible. These pieces were individually numbered on the reverse side and attached to a flat plastic forma, six at a time, using double-sided, waterproof, adhesive tape.

Grinding and polishing were carried out as follows :

(a) the sample was ground flat and even using a coarse grade of silicon carbide paper (180 grade).

(b) the sample was progressively polished using four grades of paper (220-4000 grade).

(c) the sample was polished to a 'mirror' finish using a cloth and 1-3 μm grade diamond paste, followed by 0-1 μm grade.

(d) samples were then removed from the plastic forma and adhesive tape, taking care not to scratch the polished surface.

The cleaning, degreasing and passivation were performed mostly following the procedure of Ellis [12] but with some modifications, as follows :

(a) the samples were placed in a stainless steel holder to protect the surfaces from contaminants introduced by constant handling. They were then placed in a beaker of AR 2-propanol and heated to just under boiling (i.e. 80°C for 60 minutes).

(b) following a change of 2-propanol the samples were treated in an ultrasonic bath for 15 minutes.

(c) a rinse in distilled water followed before etching in a HF/HN03 1:9 mixture for 10 seconds.

(d) once the etch was completed the samples were rinsed sequentially in distilled water, 2-propanol and a final rinse with distilled water, before being blown dry in a high purity N_2 gas stream.

The stainless steel substrates were now ready for passivation.

3.2.2. Stainless steel substrate passivation

One of the important criteria for the choice of substrate is that it forms a passive layer with respect to the pyrolytic decomposition of silanes. Many papers (see Ellis [12]) suggest that although stainless steel itself is not passive it can be made so by heating in oxygen to form a passivating oxide layer on the surface.

Passivation of the substrates had been performed by the following technique, until late October 1986 :

(a) the samples were passivated by heating in air on a clean hot plate surface at 220°C (preheated) for 20 minutes.

(b) the heater was then switched off and the samples were allowed to cool to room temperature on the hot plate for one hour.

(c) each of the samples was then removed from the hot plate and blown dry in a high purity N_2 stream to remove any dust.

Recently passivation has been carried out in a dust-free laminar flow cabinet and the last part of this step has been dropped.

The stainless steel substrates were then ready for placing in the CVD deposition chamber and were stored in the dust-free, moisture-free atmosphere of a dessicator before use.

3.2.3. Optimisation of passivation conditions

Electrical measurements performed by Dr. John Livingstone at the University of Western Australia showed that although our films, after fabrication into Schottky barrier devices, gave promising open circuit voltages, the short circuit current densities obtained were below what was needed. Four reasons were suggested for this behaviour - (1) shunt leaks, (2) high series resistance, (3) recombination traps, (4) low collection efficiency.

It was thought that 1, 3 and 4 were less significant or could be overcome by methods such as the application of anti-reflection coatings. The high series resistance was thus considered to be the most serious obstacle to raising the current density. To investigate the possible cause of this problem and to seek an understanding of the interaction of the substrate with the a-Si:H film, an XPS depth profile was carried out by Chris Lund and Craig Klauber at CSIRO, Bentley on thin fringe (0.1 μm) samples of a-Si:H on both 304 and 316 stainless steel substrates. The samples were analysed using MgKα X-rays at 300 W and 2.8 kV, with a channeltron pass energy of 50 eV

constant analyser energy (CAE). Etching was achieved by argon ion bombardment at an energy of 10 keV and a focussing energy of 4.8×10^{-7} m bar. This resulted in an ion current of 110 μA. The results of these profiles can be seen in Figs. 3.1 and 3.2.

The composition and morphology of the films will be discussed in Section 4.1. There are however several points of interest in these Figures which relate to substrate passivation, preparation and optimisation, and these will be discussed here.

As can be seen from Figs. 3.1 and 3.2, an insulating oxide layer occurs at both surfaces of the a-Si:H film. There is a thin (≈130 Å) oxide layer on the surface exposed to air and a second much thicker (≈700 Å) oxide layer between the a-Si:H film and the stainless steel substrate, due to the passivation. It is these two oxide layers that are seen as the most likely source of the high series resistance. The thicknesses quoted in Figs. 3.1 and 3.2 are based on the thicknesses of two red fringes as visible on the surface of the film, and all other measurements are based on a sputtering rate of 20 Å/min, which was derived from the above thickness divided by the total sputtering time.

The top oxide layer cannot be avoided when using the present system but it is easily removed when applying an anti-reflection coating. Therefore, it was decided to concentrate on reducing the thicker passivation layer at the metal surface.

To ascertain the effect on the electrical properties, and in particular the current density of changing the thickness of the passivating layer, an optimisation procedure was followed in which the passivation conditions only were changed and electrical measurements were performed. Four objectives were set for the experiment :

(1) to identify any effects in samples containing a range of oxidation times on similar substrates with films deposited under identical conditions,

(2) to determine whether the type of stainless steel used (304 or 316) affects the junction resistance,

(3) to determine whether the post-deposition annealing affects the hydrogen content of the films,

(4) to determine the effect of passivating the stainless steel with PO Cl_3 rather than O_2.

For these experiments, passivation was carried out in one of three ways :

(1) Passivation, as in Section 3.2.2. This approach was taken as our standard as these were the conditions under which most samples until this time had been passivated. This approach was close to that recommended by Ellis [12].

(2) Heating in air at 220°C for times ranging from 20 to 1 minute, following which the substrate was quickly removed from the heat and allowed to cool to room temperature in air.

(3) Exposure to air at room temperature for times ranging from 24 to 1 hour. These samples were prepared by etching (steps 1 - 8 in Section 3.2.2. × hours before deposition) and then left in a dessicator at room temperature until deposition.

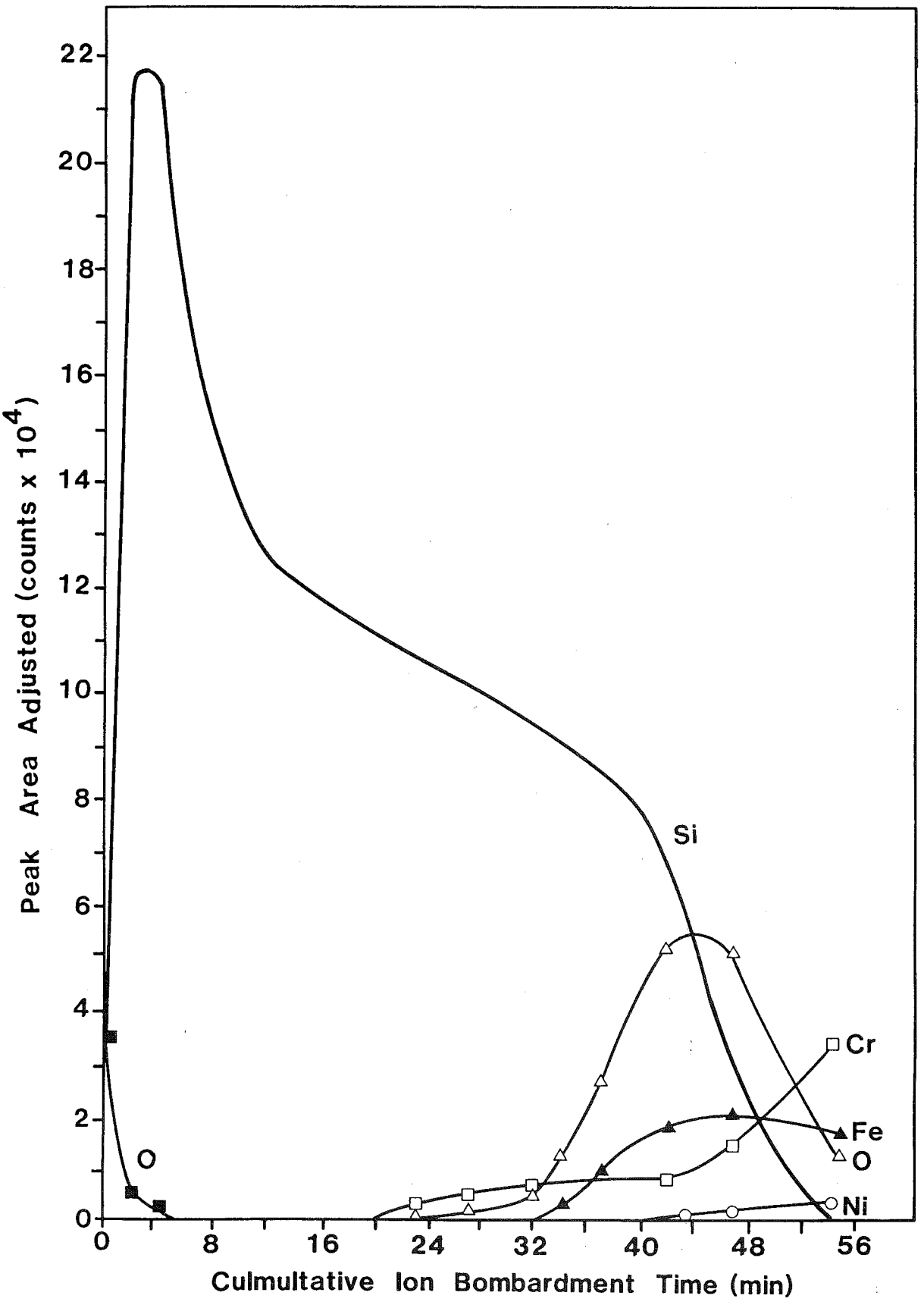

FIGURE 3.1 Auger depth profile of thin film a-Si:H on 304 stainless steel with standard passivation.

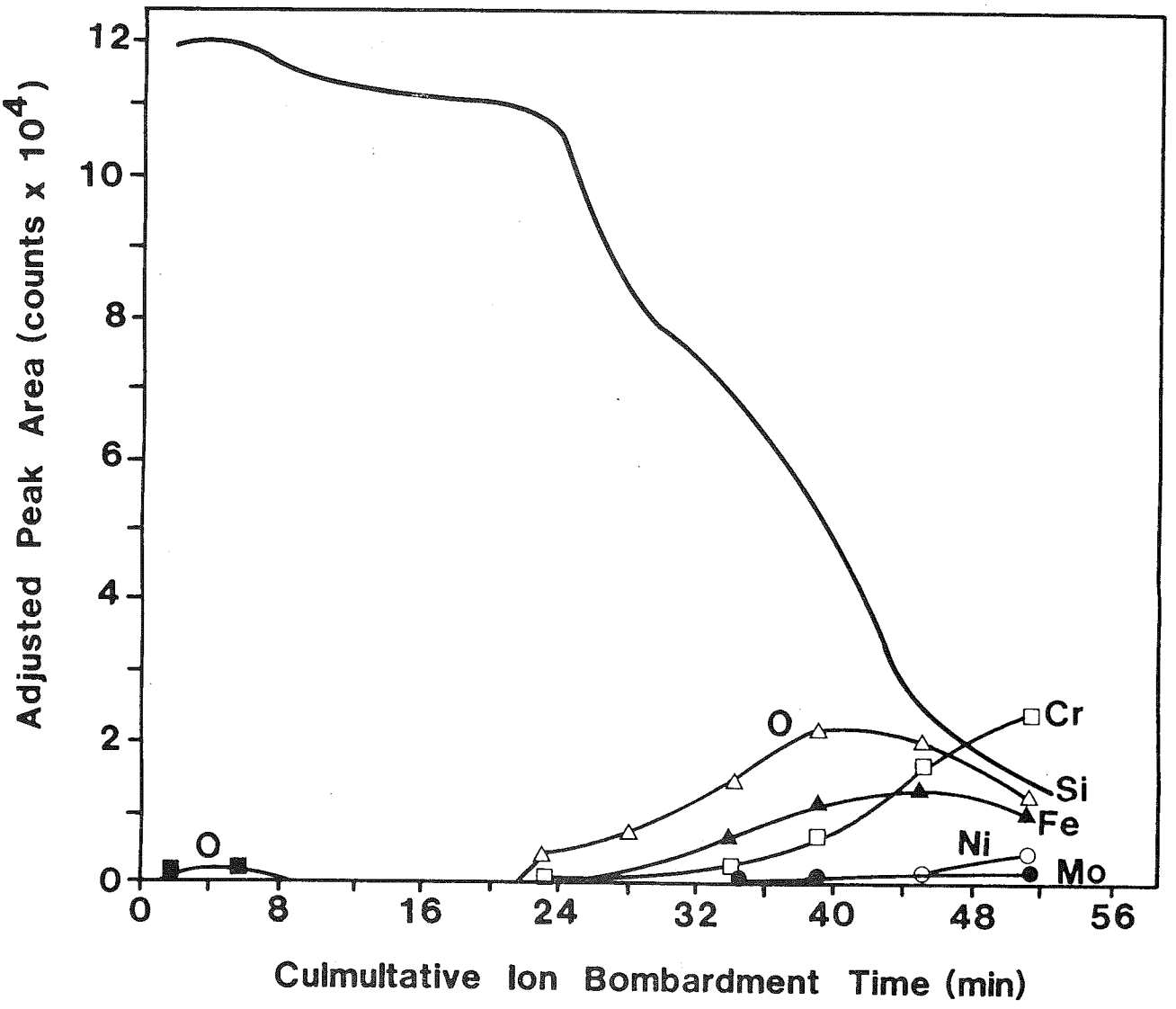

FIGURE 3.2 Auger depth profile of thin film a-Si:H on 316 stainless steel with standard passivation.

For the samples with low passivation times the final etch was completed on the day they were required, using substrates which had been left overnight between steps 6 and 7 (rinsed and dried).

Samples labelled unpassivated were etched and dried and then placed in the CVD chamber as soon as possible thereafter (typically several minutes).

Amorphous silicon was deposited under the standard conditions, i.e. block temperature 430°C, He carrier gas, flow rate 500 mL/min and no doping. This yielded films varying from about 6 μm to about 3 μm in thickness (as measured by I.R.) with varying, controlled passivation times.

Post annealing was performed by heating for a further 77 minutes at 430°C after the deposition had finished and the carrier gas had been changed from helium to hydrogen.

Electrical measurements were carried out by Dr. John Livingstone, as outlined in Section 4.5. These results, along with passivation conditions, are tabulated in Table 3.1.

The conclusions that can be drawn from these results are :

(a) There appears to be no advantage in long passivation times or for passivation at higher temperatures. Our preliminary conclusions, based on these results and several successful attempts to make cells with little or no passivation, suggest that minimal passivation (or just standing in air) is as good, both electrically and chemically, as the longer or higher temperature passivations. This is contrary to the conclusions of other researchers [12]. Further depth profiling is being undertaken to examine the thickness of the oxide layer for various passivation times to help determine the best approach and whether there is an optimal lower limit to the thickness of the oxide film.

(b) There also appears to be no advantage in using 316 or 304 stainless steel as both seem to have a Fe, Cr surface with little Ni or Mo at the surface (see Figs. 3.1 and 3.2). Depth profiles of stainless steel substrates passivated at room temperature for 12 hours, without deposition (Figs. 3.1 and 3.2), show that the surfaces consist mostly of iron and chromium oxides with nickel and molybdenum in small atom percentages. This is not the case in the bulk where the alloy elements assume their proper proportions. Based on this and the electrical results it seems clear that there is no advantage in changing from 304 SS to 316 SS in the hope of obtaining a more favourable junction resistance. It was also noticed that 316 devices tended to degrade more readily with post measurement annealing, which could be due to impurity migration.

    Similar electrical and depth profiling investigations are being undertaken on 321 SS (which has a titanium enrichment) to assess its suitability as a substrate.

(c) Post-deposition annealing at deposition temperatures seemed to have a beneficial effect on the open circuit voltages of some of the cells. For the thicker films the consistency of the current density is also improved over samples not similarly treated. Further work is in progress to explain and optimize the post-deposition annealing process.

3.2.4. $POCl_3$ on stainless steel

$POCL_3$ is widely used in the semi-conductor industry as a means of n^+ doping the surface of crystalline silicon.

By treating the surface of the stainless steel substrates in $POCl_3$ in a furnace at 800°C before deposition of the amorphous silicon layer, we hoped to introduce a slight n^+ doping to the back surface of the a-Si:H film and to passivate the stainless steel surface before deposition. That is, we hoped to achieve both a good chemical and electrical contact between the substrate and the amorphous film.

As $POCl_3$ seemed to passivate the stainless steel surface, two tests were carried out to ascertain its success in improving the electrical contact. The first of these were a set of electrical tests, where a-Si:H was deposited on the $POCl_3$ treated substrates. These films were fabricated into Schottky devices and compared with a set of samples passivated normally and deposited under similar conditions. The second test was a depth profile through the metal/amorphous silicon junction using XPS.

For the XPS studies the experimental procedure was the same as that described previously in Section 3.2.3.

The oxygen/phosphorus ratio (atomic %) does not decrease with increasing time (depth) of sputtering of the stainless steel surface. This suggests that the surface is not simply covered with oxide and phosphide but that in fact the entire surface is coated with a phosphorus/oxygen compound. This means that the only phosphorus present is there as a phosphate and not as a phosphide. The decrease in phosphorus at the end of the profile, when oxygen remains constant, could be explained by partial conversion of the oxide film on the stainless steel layer by the $POCl_3$. As can be seen in Fig. 3.3, there is no chlorine present.

A layer structure like the one described above would lead to an insulating layer between the substrate and the a-Si:H film. This would reduce the electrical conductivity rather than enhance it, as we had hoped.

To further investigate the effect of $POCl_3$ passivation on the electrical properties of a-Si:H cells, two $POCl_3$ treated samples were tested. As can be seen from Table 1, the current density is quite low when compared with similar 304 SS samples passivated in air. This seems to confirm the results predicted by XPS profiling. Although there are not enough samples to provide a complete confirmation that an insulating rather than a conducting layer was formed, the trend, especially in light of the XPS profiling, seems to suggest that this is the case.

The V_{OC} (max) values from the $POCl_3$ treated samples are comparable with the air-passivated samples. The V_{OC} (min) values were consistent and amongst the highest of all the samples. This indicates that $POCl_3$ treatment achieves a good chemical passivation (i.e. a uniform film), however this advantage is outweighed by the severe reduction in current density. Therefore, $POCl_3$ treatment as performed here is not suitable as a means of passivating the stainless steel.

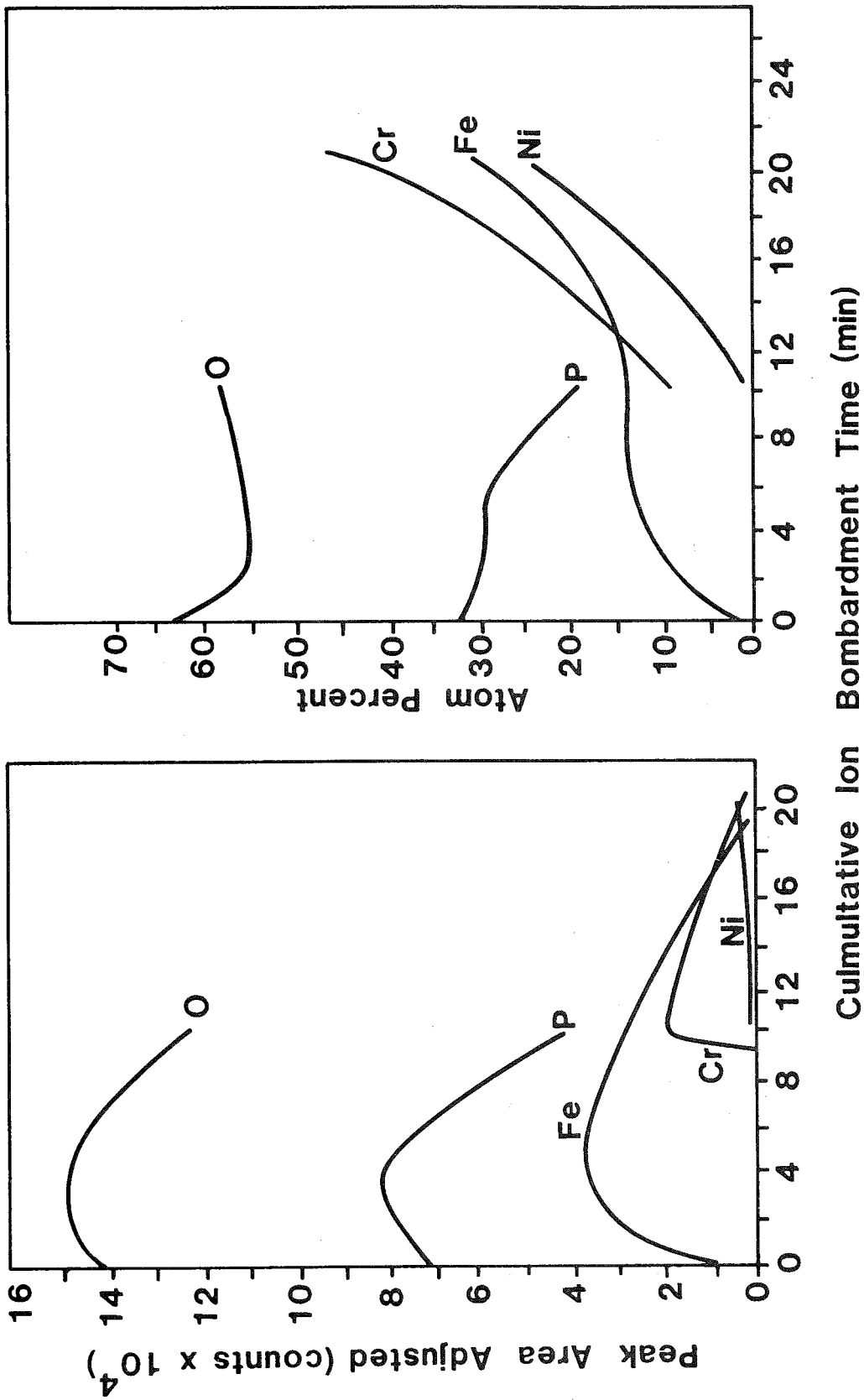

FIGURE 3.3 Auger depth profile of 304 stainless steel after treatment with PO Cl_3

3.3. Other Substrates

For the reasons given above, stainless steel has been the main substrate used, however investigations into the suitability of other substrates have also been undertaken. Deposits have been made onto crystalline silicon, glass, copper, silver, titanium, tantalum and indium tin oxide, either in the bulk or as films on glass.

Glass and crystalline silicon substrates have been used only for optical measurements as they do not provide an ohmic back contact to the film.

Glass substrates are cleaned prior to deposition using the following procedure :

(1) rinse in chromic acid,

(2) place in Decon 90 in an ultrasonic bath for 15 minutes,

(3) clean in ultrapure water in an ultrasonic bath for 15 minutes,

(4) allow to dry in air.

The intrinsic crystalline silicon wafers are also cleaned prior to deposition, as follows :

(1) etch in hydrofluoric acid for 30 seconds,

(2) rinse in ultrapure water,

(3) dry in a stream of high purity N_2.

Of all the other substrates, only titanium and tantalum gave good adherent films. Copper and indium tin oxide reacted with the deposited silicon and silver diffused through the film.

Although patches of specular a-Si films were occasionally obtained, copper substrates seemed to promote the formation of a black, or greenish, powdery layer which did not adhere to the polished surface. Aluminium on glass reacted with the silane gas mixture, clearly forming a milky white deposit which was unsuitable for analysis. Silver on glass migrated through the a-Si:H layer, forming metallic globules on the surface.

Of all the metal films on glass which we tried, only titanium and tantalum gave uniform films of satisfactory appearance. Further investigation of these, as well as chromium and molybdenum, are being carried out both on glass and as thin films on stainless steel.

4. CHARACTERISATION OF a-Si:H FILMS

4.1. Morphology

Films of a-Si:H of varying visual appearance have been studied by scanning electron microscopy (SEM). In general, visually clean specular films show relatively smooth featureless amorphous deposits (Figs. 4.1 and 4.2). At high magnification the surfaces tend to show an 'orange peel' appearance (Fig. 4.3). Some of the surfaces have on them a number of smooth spherical globules 1-4 μm in diameter which do not appear to be part of the surface yet resist attempts to remove them by compressed air or NaOH treatment. They may have their origin in the dusty deposits observed in the cooler parts of the CVD reactor system.

Films that appear dull, generally grey or even black show a high density of polycrystalline whiskers growing on the surface when viewed under the SEM (Fig. 4.4). These are attributed to polycrystalline silicon and have been observed on both stainless steel substrates and copper substrates. A third form that the deposit may take has an opalescent visual appearance and under the SEM the surface is rough and appears to be formed from a large number of close-packed spheres (Fig. 4.5).

Both specular and dull films were checked for crystallinity using X-ray diffraction. There was no evidence of this in the specular films but the dull films showed some crystallinity, confirming the SEM observations.

4.2. Optical Measurements

4.2.1. Measurement of the refractive index and thickness of thin films using optical techniques

For a thin film of thickness d_1 and refractive index n_1 on a substrate of refractive index n_2 illuminated at normal incidence (Fig. 4.6)

$$n_0 < n_2 < n_1$$

The path difference between 1 and 2 is $2d_1$ where d_1 is thickness of film. This produces a phase difference of

$$2\pi \left(\frac{2d_1}{\lambda_1} \right)$$

where λ_1 is the wavelength of light in the film, or

$$2\pi \left(\frac{2d_1 n_1}{\lambda_0} \right)$$

where λ_0 is the wavelength of light in air and n_1 is the refractive index of the film. When the path length difference $2d_1n_1$ is zero or a whole number of wavelengths, there is destructive interference and less light is reflected. When the path length difference is an odd number of half wavelengths, constructive interference is obtained and more light is reflected. Hence, if we illuminate the film with light of varying wavelength, we get a series of maxima and minima in the transmitted light. (See Fig. 4.7).

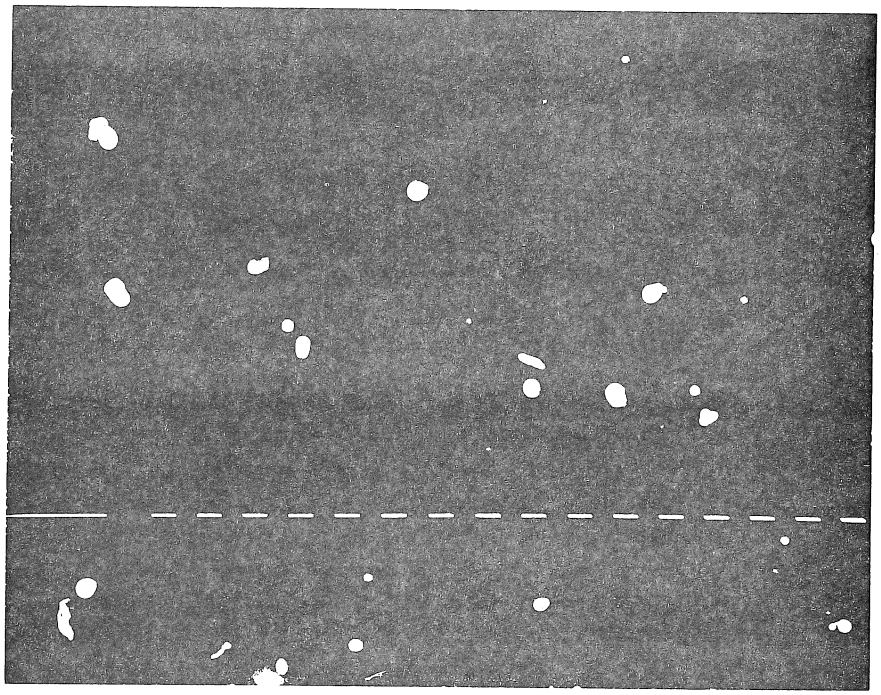

FIGURE 4.1 SEM of specular film X320

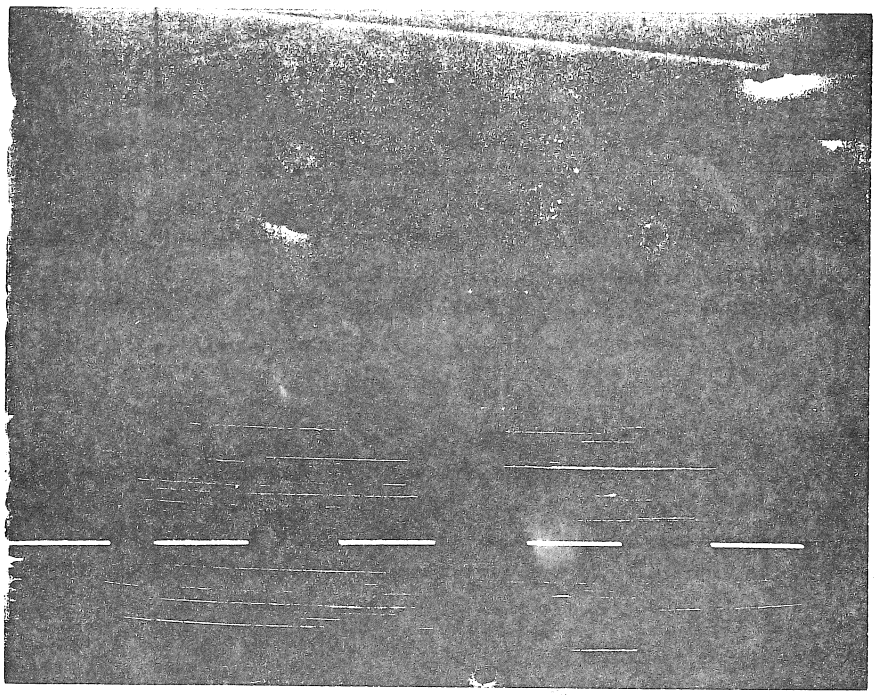

FIGURE 4.2 SEM of specular film X1250

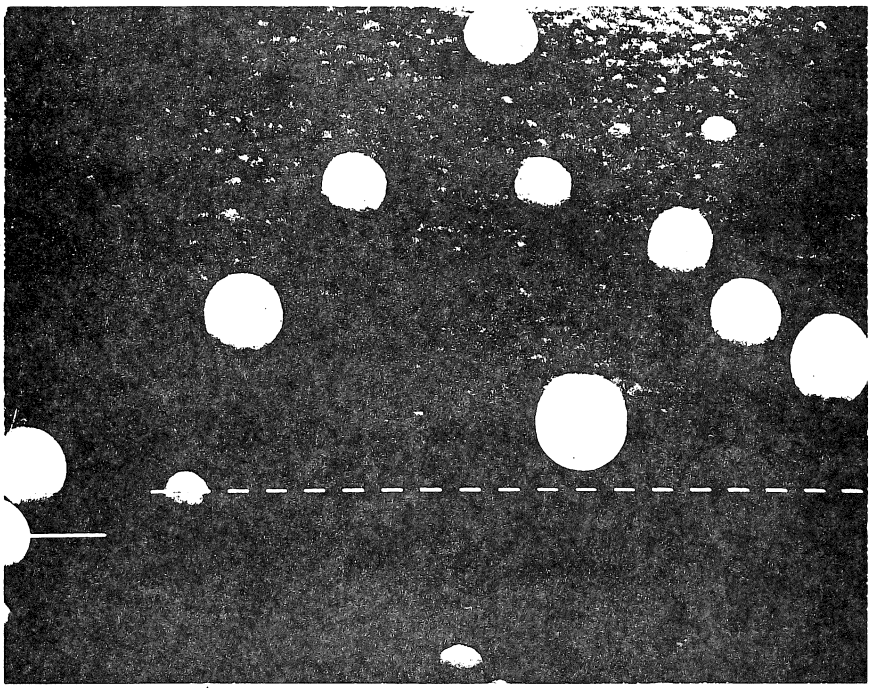

FIGURE 4.3 SEM of specular film X2500

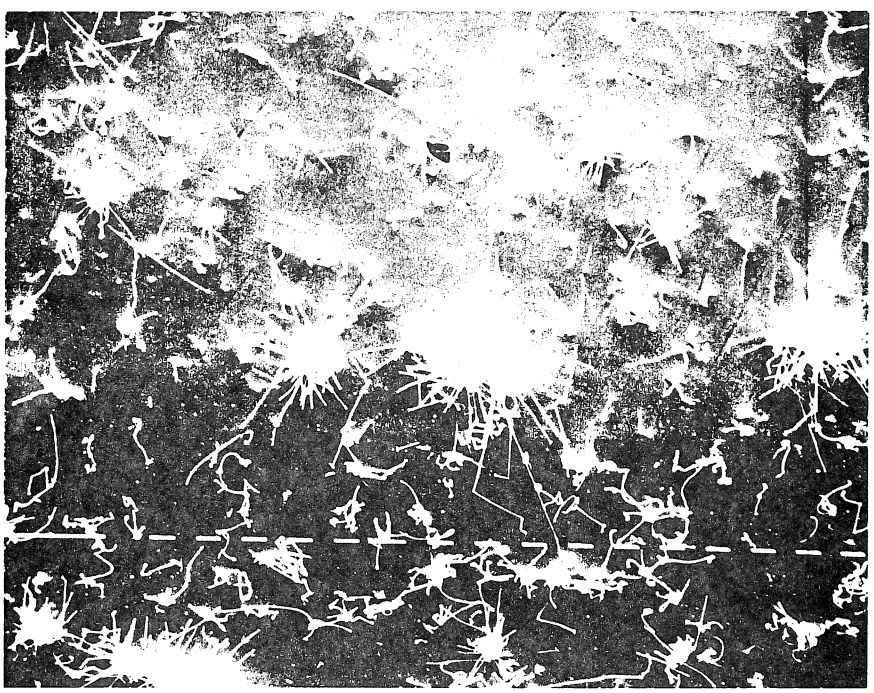

FIGURE 4.4 SEM of dull grey film X320

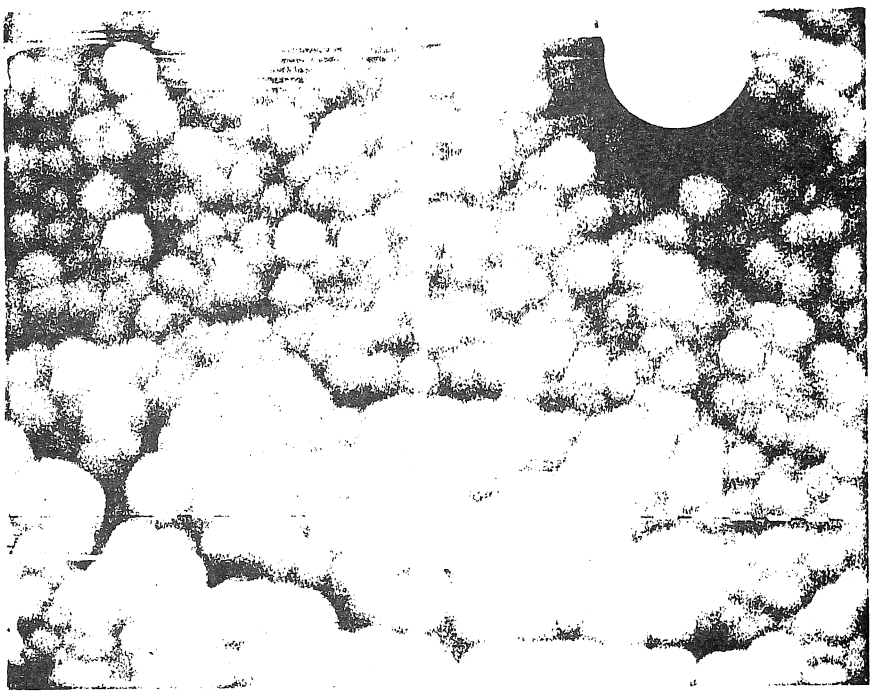

FIGURE 4.5 SEM of opalescent film X2500

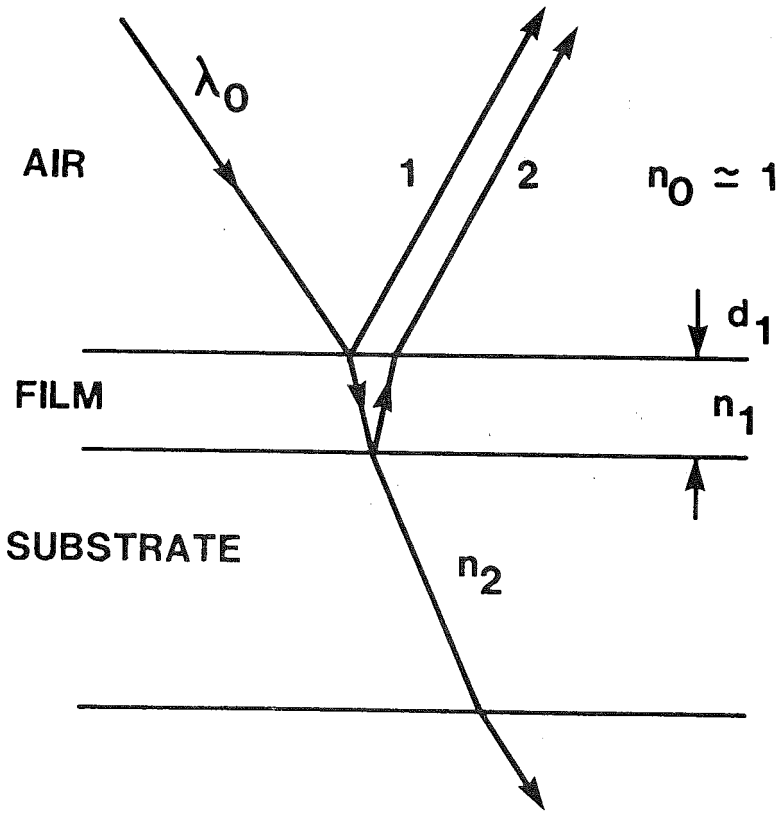

FIGURE 4.6 Refraction and reflection of light from a thin film on a dielectric substrate ($n_0 < n_2 < n_1$).

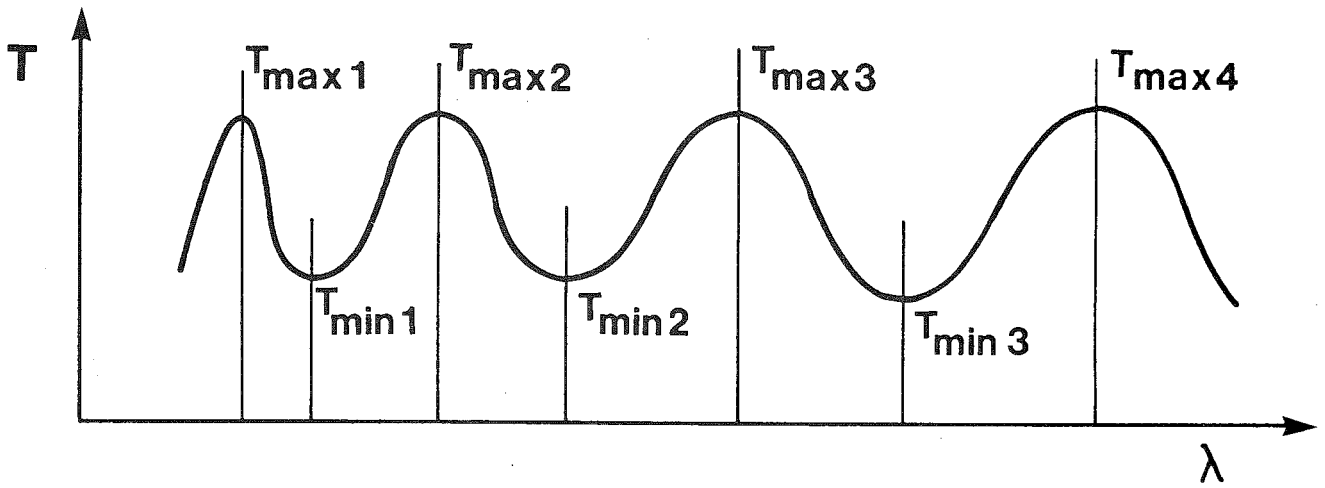

FIGURE 4.7 Predicted transmitted light intensity T through an ideal thin film as a function of wavelength λ.

The thickness of the film can be found from either

$$d_1 = \frac{1}{2n_1} \left| \frac{\lambda_{min1}\ \lambda_{min2}}{\lambda_{min1} + \lambda_{min2}} \right|$$

$$\text{or} \quad d_1 = \frac{1}{2n_1} \left| \frac{\lambda_{max1}\ \lambda_{max2}}{\lambda_{max1} + \lambda_{max2}} \right|$$

$$\text{or} \quad d_1 = \frac{1}{4n_1} \left| \frac{\lambda_{max}\ \lambda_{min}}{\lambda_{max} - \lambda_{min}} \right|$$

where λ_{min} and λ_{max} are adjacent [13].

We need to know the refractive index to use these expressions.

If the refractive index of the film is unknown then adjacent values of T_{max} and T_{min} are used first to get the ratio

$$\rho_{T_2} = \frac{T_{max}}{T_{min}}$$

This can then be put into the expression

$$n_1 = \left[\frac{-(1+n_2^2)(1-2\rho_{T_2}) + \{(1+n_2^2)\ (1-2\rho_{T_2})^2 - 4n_2^2\}^{\frac{1}{2}}}{2} \right]^{\frac{1}{2}}$$

to obtain the refractive index of the film n_1. [14]

To avoid the tedious calculation each time, and since n_2 is a known constant, a graph of ρ_{T_2} vs n can be prepared for a range of values, enabling n_1 to be read off.

In practice, in the visible region of the spectrum, the interference fringes are superimposed on the absorption edge and a plot of transmission vs wavelength is shown in Figure 4.8.

In this case it is necessary to use the longest wavelength transmission maximum and minimum values obtained to find the refractive index. The positions of the maxima and minima are not affected and any pair may be used for the subsequent thickness determination.

A similar analysis can be applied to the measurement of films on stainless steel substrates. These are measured in the near IR using a commercial reflection attachment. Changes to the analysis are necessary in this case because the experiment is not carried out at normal incidence. Films produced have thicknesses varying from ~0.5 μm to over 4 μm and refractive indices between 3.34 and 3.60, with a mean value ~3.5 (Tables 4.1 and 4.2).

The thickness of the a-Si films was also determined by stylus displacement measurements using a surfometer SF 101. Its measurement ranges are from 0.01 to 100 micrometres. The method requires the films to be first deposited on a very flat surface (i.e. a glass slide) and then the stylus is drawn across the slide and the deposited films. A typical profile is shown in Fig. 4.9.

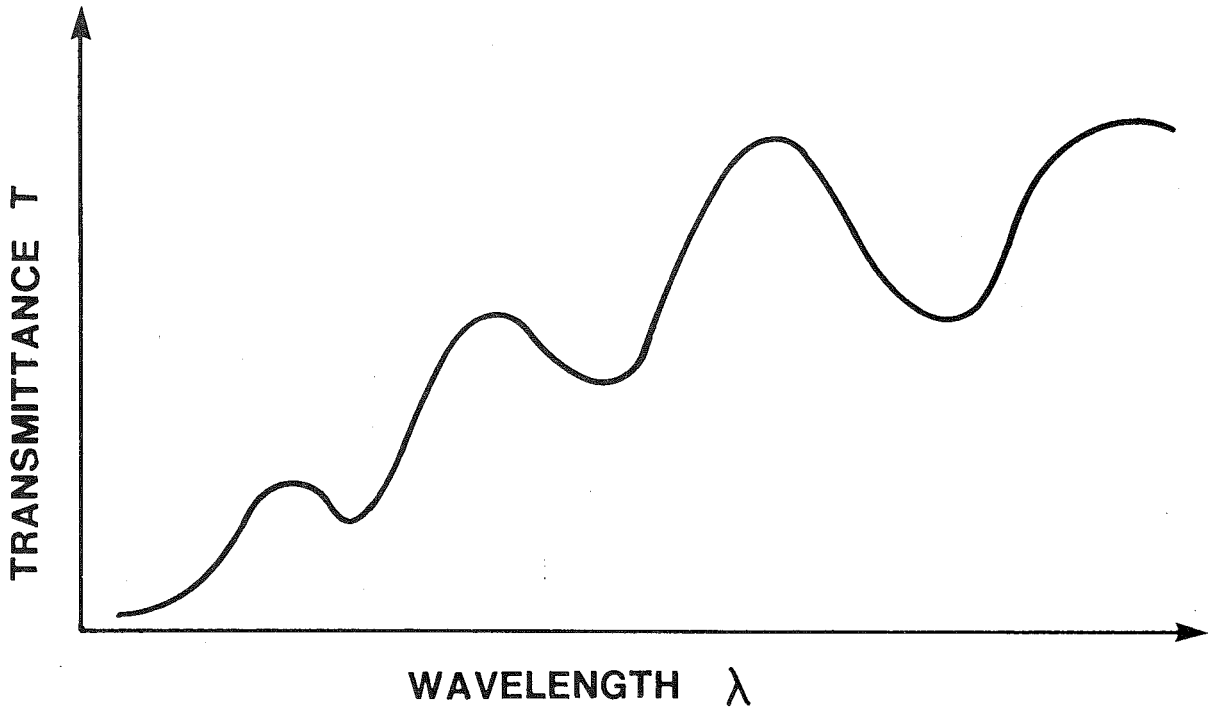

FIGURE 4.8 Actual measured transmittance T through a real thin film as a function of wavelength λ.

TABLE 4.1

Refractive Indices for a-Si:H Films on Glass Substrates

Sample	T_{max}	T_{min}	ρ_T	n_1
111	0.860	0.340	2.53	3.60
112	0.790	0.325	2.43	3.52
169	0.850	0.380	2.24	3.34
170	0.840	0.365	2.30	3.49
178	0.855	0.345	2.48	3.56
G107	0.900	0.370	2.43	3.52
G108	0.880	0.370	2.38	3.47

TABLE 4.2

Thickness and Optical Band Gap for a-Si:H Films on Glass Substrates

Sample	Ts (°C)	Flow Rate (ml/min)	Dep Time (min)	d (μm)	Growth Rate (As^{-1})	Eg (eV)
103	600	800	83	0.71	1.4	1.48
105	600	800	20	0.94	7.9	1.51
107	600	800	18	0.89	8.2	1.52
111	590	800	25	0.98	6.5	1.54
112	600	800	14	0.70	8.4	1.53
169	450	800	37	0.92	4.1	1.53
170	450	800	37	0.61	2.8	1.51
178	420	800	44	0.96	3.6	1.52
G107	400	500	85	0.67	1.3	-
G108	400	500	68	0.82	2.0	-
G109	400	500	91	1.2	2.2	1.55
G110	400	500	49	1.2	4.0	1.54
G111	450	500	76	0.82	1.8	1.57
G114	450	500	97	0.79	1.4	1.56
G115	430	500	83	0.48	0.97	1.52
G116	430	500	85	0.78	1.5	1.54
G119	430	500	90	3.5	6.4	1.45
G120*	430	500	72	3.0	7.0	1.46
G122#	380	500	90	1.1	2.1	1.42

* Phosphorus doped

Boron doped

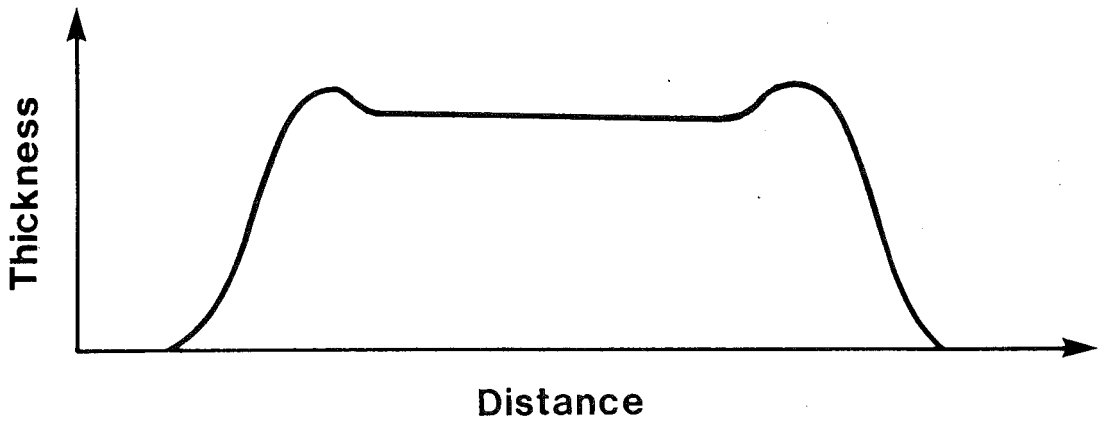

FIGURE 4.9 Thickness versus distance measurements using a surfometer on a-Si:H films.

4.2.2. The optical bandgap

From a measurement of the optical absorption coefficient, the optical bandgap of a-Si films can be deduced by using the following expression

$$(\alpha h\nu)^{\frac{1}{2}} = C_t\ (h\nu - E_{opt})$$

where α is the optical absorption coefficient, ν is the frequency of the radiation, E_{opt} is the optical gap or the Tauc gap of the material and C_t is a constant.

E_{opt} is a measure of the energy of optical transitions between extended states in the valence and conduction bands under the assumption of parabolic bands and constant matrix elements. The optical gap is obtained from the intercept of the extrapolation of the linear portion of the plot of $(\alpha h\nu)^{\frac{1}{2}}$ vs $(h\nu)$.

The optical absorption of a-Si films was measured as a function of wavelength over the visible spectrum. The set-up is shown in Fig. 4.10.

By using the relationship

$$I(x) = I(o)\ \exp\ (-\alpha x)$$

the optical absorption coefficient for the various a-Si:H films can be determined. The light source consists of a tungsten lamp which provides white light over the visible spectrum. Transmitted intensities are measured over the visible spectrum, between 270 nm and 800 nm, using the IL 700 research radiometer (International Light). The absorption coefficient, α, of the films is calculated from the ratio of the two intensity levels, I(0) and I(x).
From this plot of absorbance vs wavelength the absorption coefficient is obtained as a function of photon energy, as in Fig. 4.11.

$$\alpha = \left|\frac{\ln \log^{-1} A}{d}\right| \quad \text{and} \quad h\nu = \frac{hc}{\lambda e}\ \text{eV} = \frac{1.24 \times 10^{-6}}{\lambda}\ \text{eV}$$

A plot of $h\nu$ vs $(\alpha h\nu)^{\frac{1}{2}}$ yields essentially a straight line which can be extrapolated to cut the $h\nu$ axis. The value obtained is thus the optical band gap, according to

$$\alpha = \frac{C^2(h\nu - E_{opt})^2}{h\nu} \qquad [15]$$

Typical results are shown in Fig. 4.12.

The optical bandgap values obtained from the optical measurements were in the range 1.42 - 1.57 eV (Table 4.2). A similar value (1.6 eV) was obtained from SPV analysis.

4.3. Composition of a-Si:H Film

Samples have been investigated by XPS and AES depth profiling.

In XPS (ESCA) the specimen is irradiated with monochromatic X-rays. A photon is absorbed, with the emission of a photoelectron whose kinetic energy is equal to the energy of the incident photon minus the binding energy of the electron in the solid. The electrons come from a thin layer near the surface, typically 50 Angstrom in depth. Commercial XPS machines scan over a range typically 4 to 4000 eV. Auger electrons within this range are also recorded along with the photoelectrons. The energy spectrum can be scanned at variable rates -

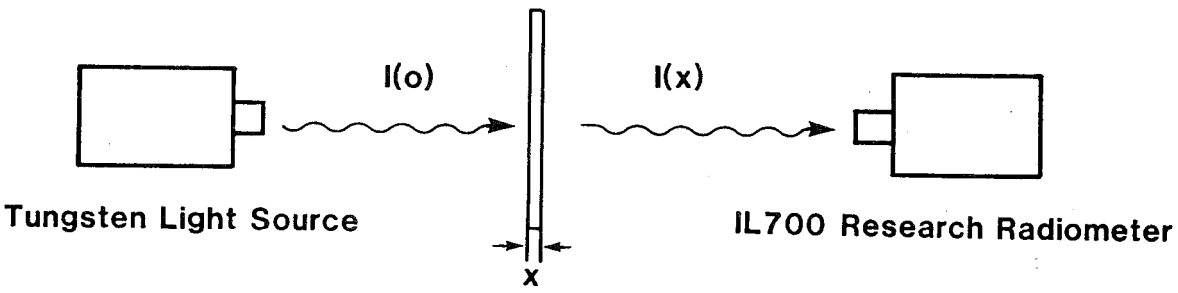

FIGURE 4.10 Arrangement for optical absorption measurements on a-Si:H films.

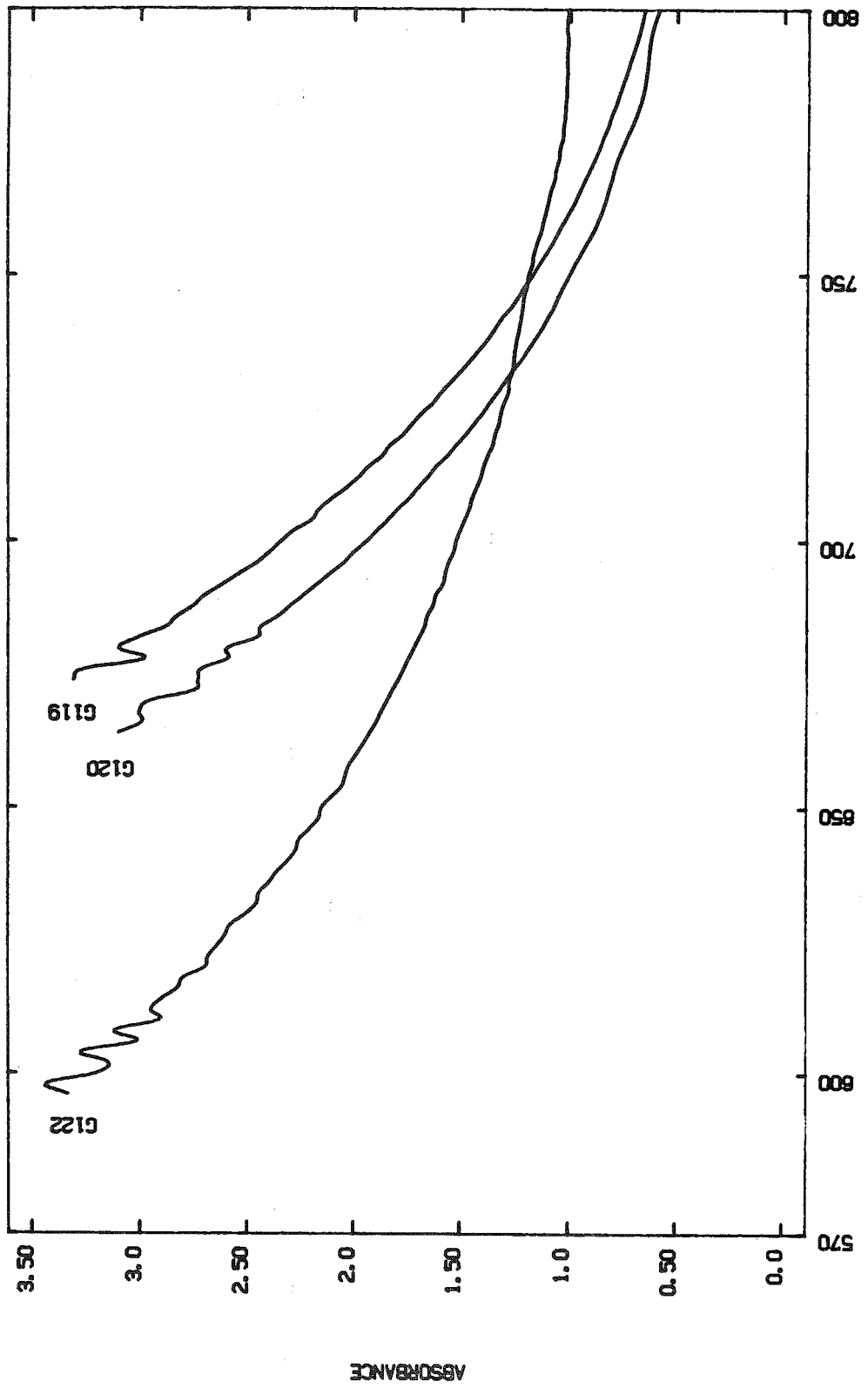

FIGURE 4.11 Visible absorption spectra for samples G119, G120 and G122.

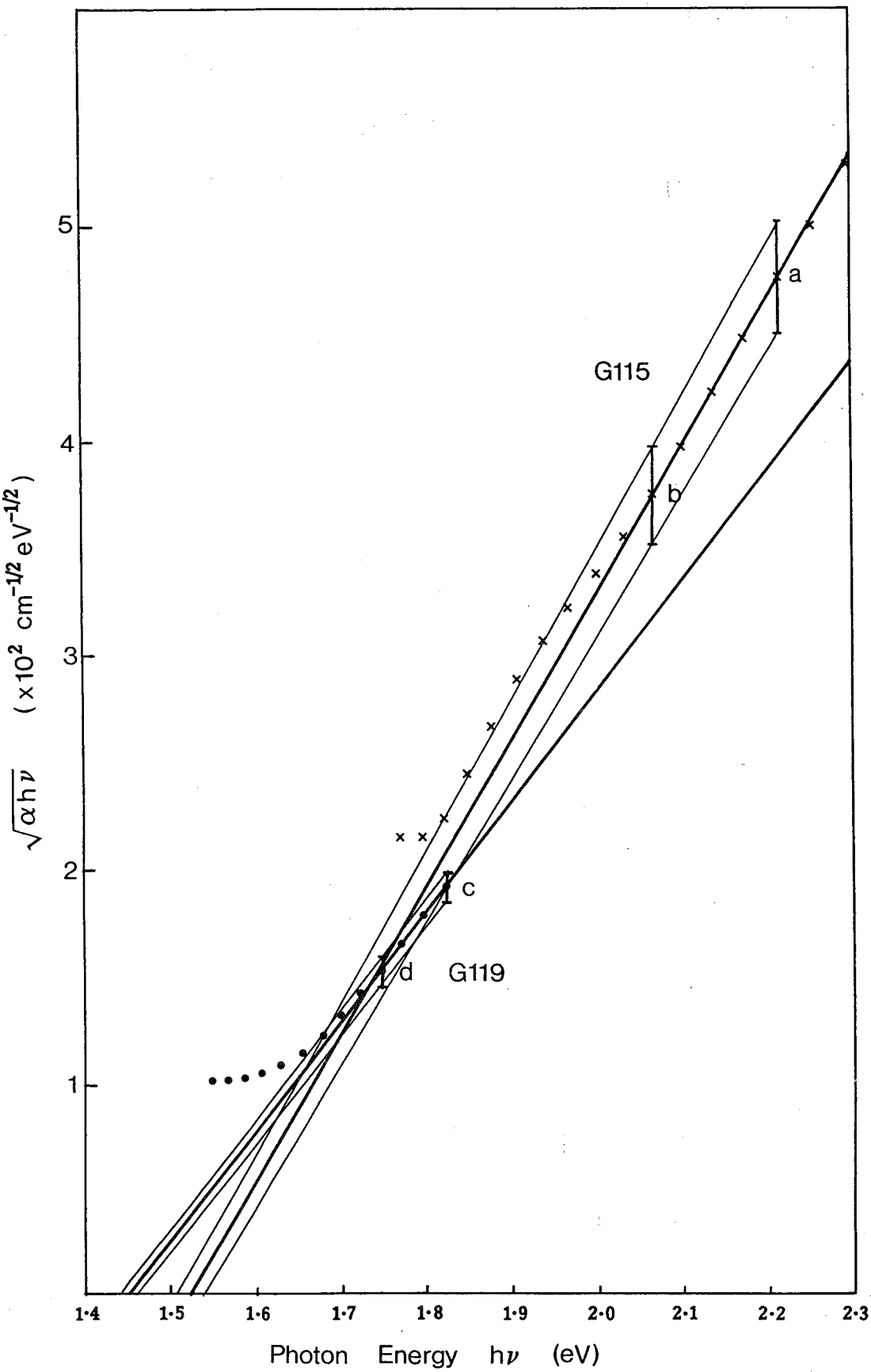

FIGURE 4.12 Tauc band gap plots for samples G115 (0.48 μm) and G119 (3.5 μm).

a rapid scan over the spectrum will indicate whether an element is present, be it free or combined, or both; a slow scan over the narrow spectral region, known and marked out for an element, will give more detailed information.

Initially a general survey was carried out on sample #631 (a glow discharge sample) using the Mg Kα X-ray band to establish a reference spectrum for the a-Si:H surface composition from a known sample. This spectrum (Fig. 4.13) showed the presence of oxygen (oxygen KLL Auger peak at 740-800 eV and 01s X-ray peak at 532 eV), nitrogen (N1s,401.6 eV) and silicon (Si2s,149.9 eV and Si2p,99.2 eV). There was also some aluminium (Aℓ2p,73.1 eV and Aℓ2s,17.7 eV) present. The boron peak expected was not clearly distinguishable from the background.

General surveys were carried out on samples #242 (intrinsic), #317 (P-doped) and #353 (unknown doping) using the Mg Kα X-ray band and all samples were CVD samples. For the intrinsic sample there were three features distinctly different from sample #631. Firstly, there was no (N1s,401.8 eV) nitrogen peak distinguishable above the background in the CVD sample (Fig. 4.14). Secondly, the carbon (C1s,284 eV) peak was greatly diminished. This suggested some carbon contamination on the surface layer of the a-Si:H but not the large amount of carbon in the bulk, as in the G.D. This is what would be expected as the G.D. sample had an approximately equivalent stoichiometric amount of carbon incorporated in the bulk to change the optical properties of the film. This explains the large carbon peak in Fig. 4.13. Furthermore, the small carbon peak in Fig. 4.14 was later confirmed by further Ar ion bombardment to be only surface contamination. The final difference that can be seen between the two spectra is the plasmons at 187, 202, 134 and 117 eV (Fig. 4.15) due to excitations from deeper levels being accompanied by an inelastic excitation of plasmons. These are normal for the XPS spectrum of silicon. That these were not visible in the G.D. spectrum is presumably a reflection of the difference in lattice structure caused by the incorporation of carbon in the a-Si:H lattice.

Both of the doped samples reflected the features found in the intrinsic sample (Figs. 4.16 and 4.17). However, due to the plasmon peaks lying in the range 187 to 117 eV, which overlaps the X-ray phosphorus and boron peaks at 189, 132 and 188 eV respectively, they were indistinguishable from the plasmons. Because the X-ray peaks were unusable for either quantitative or qualitative work, more detailed scans of the region 700-1200 eV (Binding energy) were carried out to investigate the possibility of using the Auger electron peaks for phosphorus and boron detection. Initial scans of both #317 and #353 showed no phosphorus or boron peaks in the region where they were expected. Even more detailed scans of the "as introduced" surface showed no distinct peaks.

Because electronic testing has revealed that phosphorus is indeed present, the samples were then ion bombarded for five minutes, at an energy of 10 kV with a focus energy of 5kV, in the hope of removing the oxide layer and carbon contamination from the surface to reveal the phosphorus doping. A general Mg Kα survey after bombardment revealed the following :

(1) The carbon present in Fig. 4.14 was only surface contamination as the C1s,284 eV peak disappeared (Fig. 4.18).

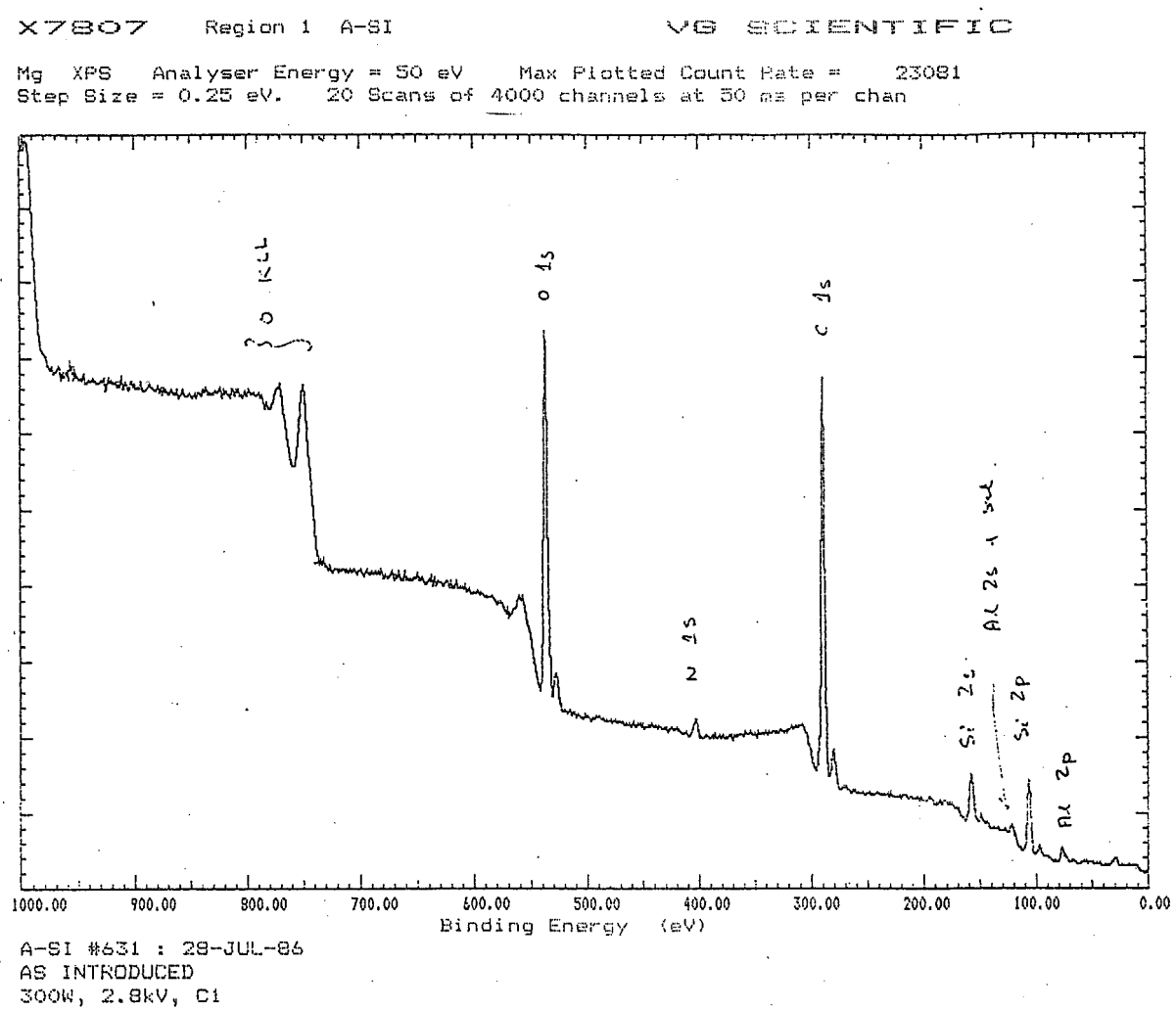
X7807 Region 1 A-SI
VG SCIENTIFIC
Mg XPS Analyser Energy = 50 eV Max Plotted Count Rate = 23081
Step Size = 0.25 eV. 20 Scans of 4000 channels at 50 ms per chan
O KLL
O 1s
C 1s
Al 2s
Si 2s
Si 2p
Al 2p
1000.00
900.00
800.00
700.00
600.00
500.00
400.00
300.00
200.00
100.00
0.00
Binding Energy (eV)
A-SI #631 : 28-JUL-86
AS INTRODUCED
300W, 2.8kV, C1

FIGURE 4.13

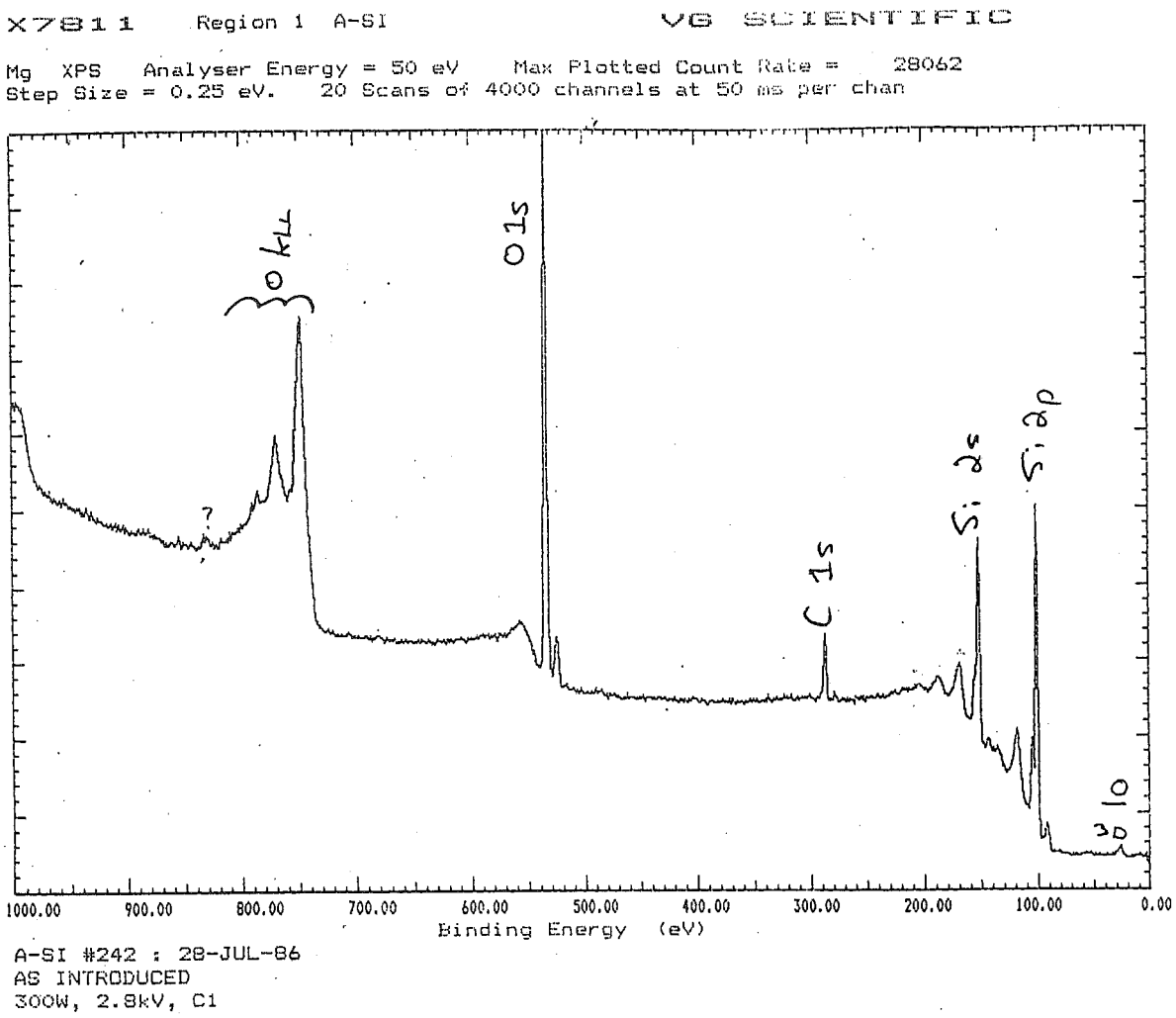
X7811 Region 1 A-SI
VG SCIENTIFIC
Mg XPS Analyser Energy = 50 eV Max Plotted Count Rate = 28062
Step Size = 0.25 eV. 20 Scans of 4000 channels at 50 ms per chan
O KLL
O 1s
C 1s
Si 2s
Si 2p
?
1000.00
900.00
800.00
700.00
600.00
500.00
400.00
300.00
200.00
100.00
0.00
Binding Energy (eV)
A-SI #242 : 28-JUL-86
AS INTRODUCED
300W, 2.8kV, C1

FIGURE 4.14

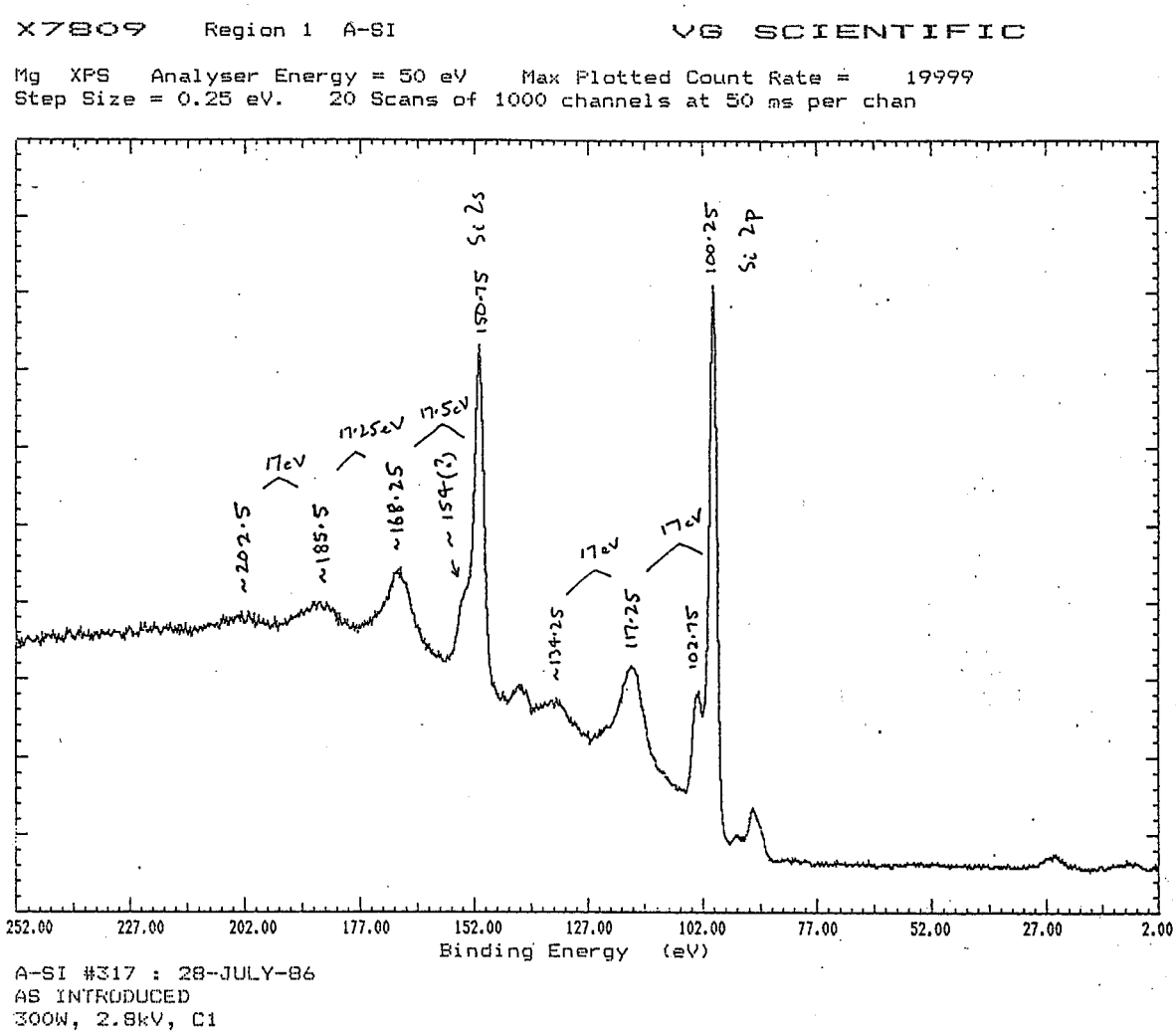
X7809 Region 1 A-SI
VG SCIENTIFIC
Mg XPS Analyser Energy = 50 eV Max Plotted Count Rate = 19999
Step Size = 0.25 eV. 20 Scans of 1000 channels at 50 ms per chan
~202.5
17eV
~185.5
17.25eV
~168.25
17.5eV
~154(?)
150.75
Si 2s
~134.25
17eV
117.25
17eV
102.75
100.25
Si 2P
252.00
227.00
202.00
177.00
152.00
127.00
102.00
77.00
52.00
27.00
2.00
Binding Energy (eV)
A-SI #317 : 28-JULY-86
AS INTRODUCED
300W, 2.8kV, C1

FIGURE 4.15

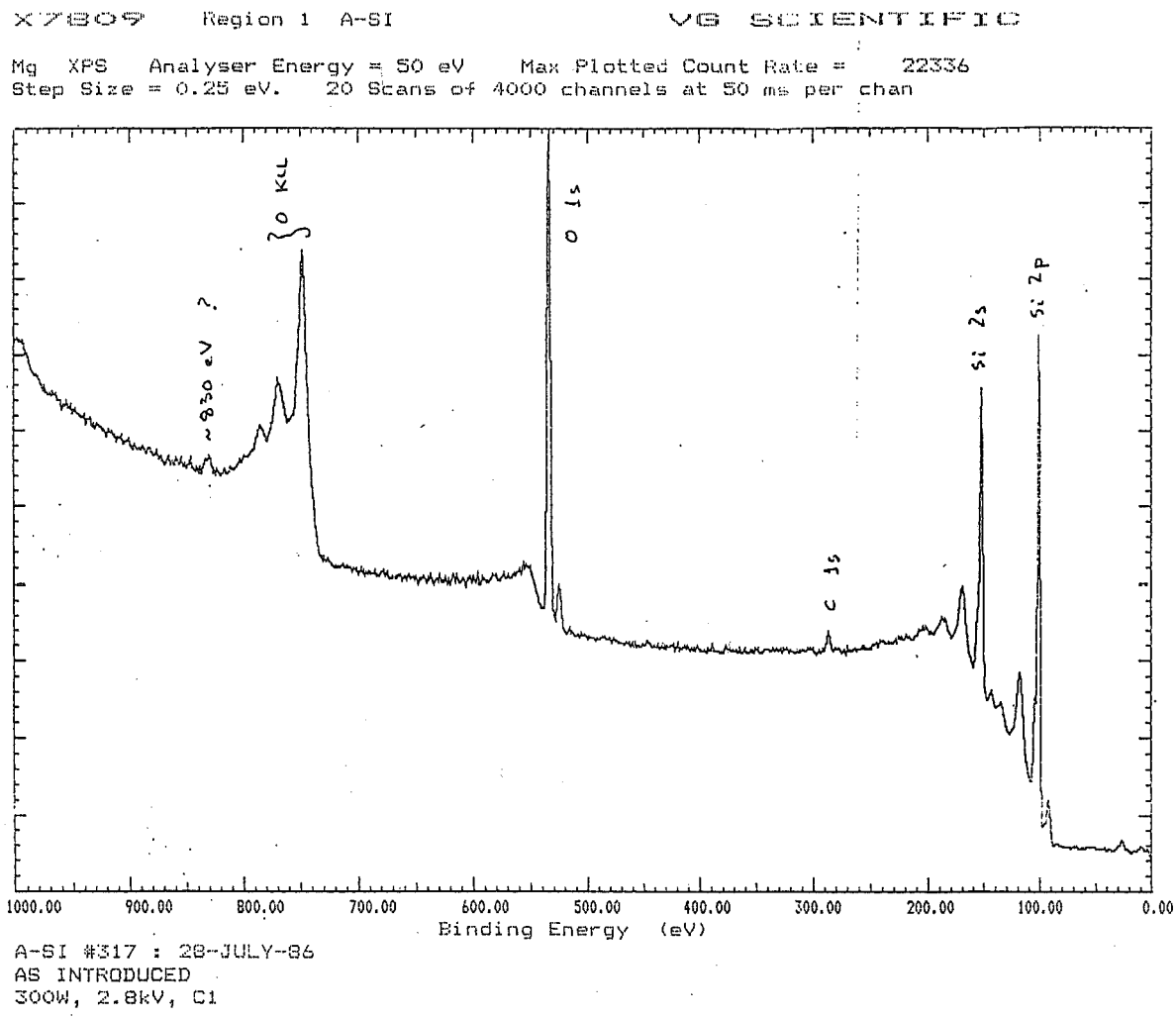
X7809 Region 1 A-SI
VG SCIENTIFIC
Mg XPS Analyser Energy = 50 eV Max Plotted Count Rate = 22336
Step Size = 0.25 eV. 20 Scans of 4000 channels at 50 ms per chan
~830 eV ?
~O KLL
O 1s
C 1s
Si 2s
Si 2p
1000.00
900.00
800.00
700.00
600.00
500.00
400.00
300.00
200.00
100.00
0.00
Binding Energy (eV)
A-SI #317 : 28-JULY-86
AS INTRODUCED
300W, 2.8kV, C1

FIGURE 4.16

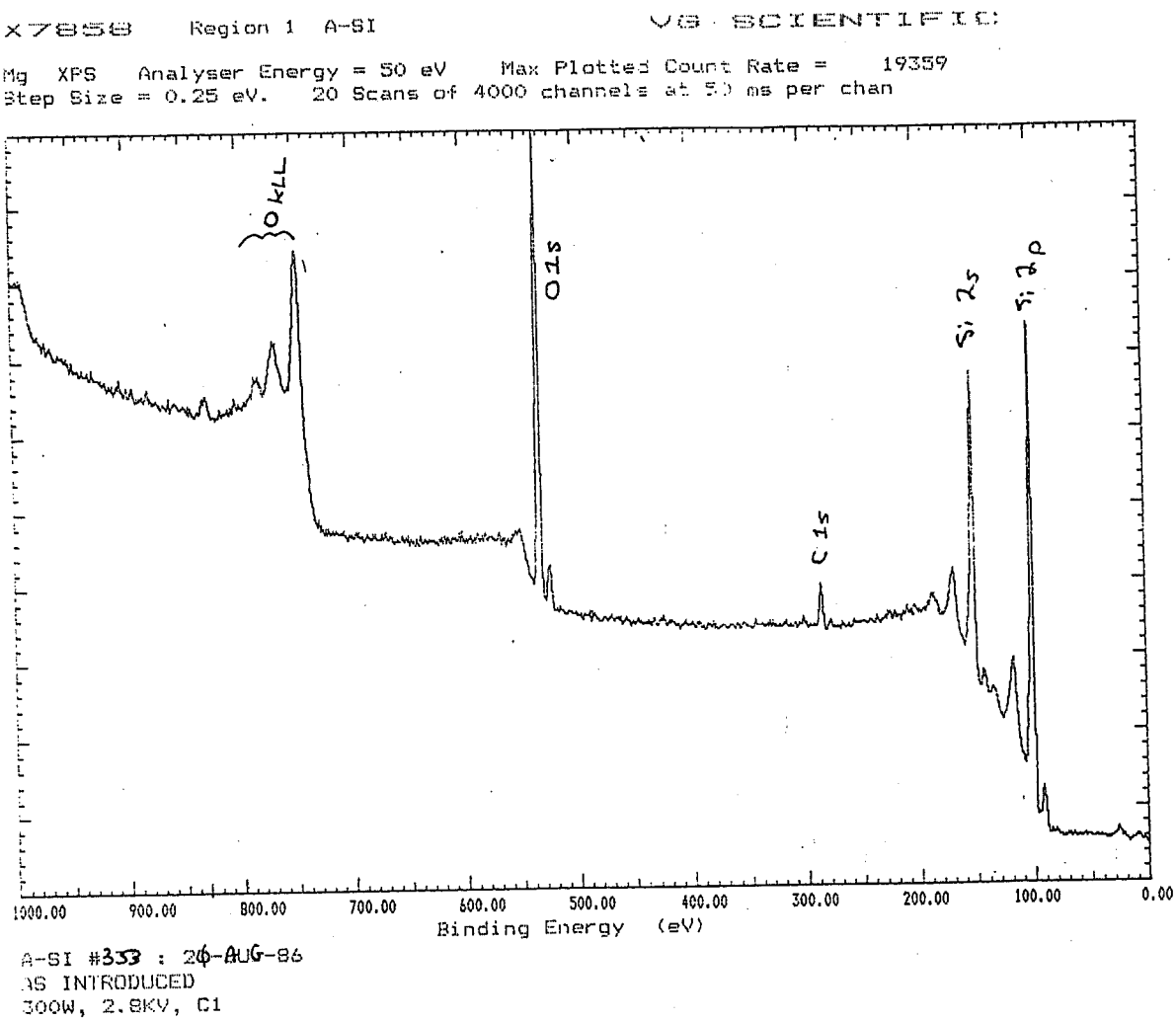
X7858 Region 1 A-SI
VG SCIENTIFIC
Mg XPS Analyser Energy = 50 eV Max Plotted Count Rate = 19359
Step Size = 0.25 eV. 20 Scans of 4000 channels at 50 ms per chan
O KLL
O 1s
C 1s
Si 2s
Si 2p
1000.00
900.00
800.00
700.00
600.00
500.00
400.00
300.00
200.00
100.00
0.00
Binding Energy (eV)
A-SI #333 : 26-AUG-86
AS INTRODUCED
300W, 2.8KV, C1

FIGURE 4.17

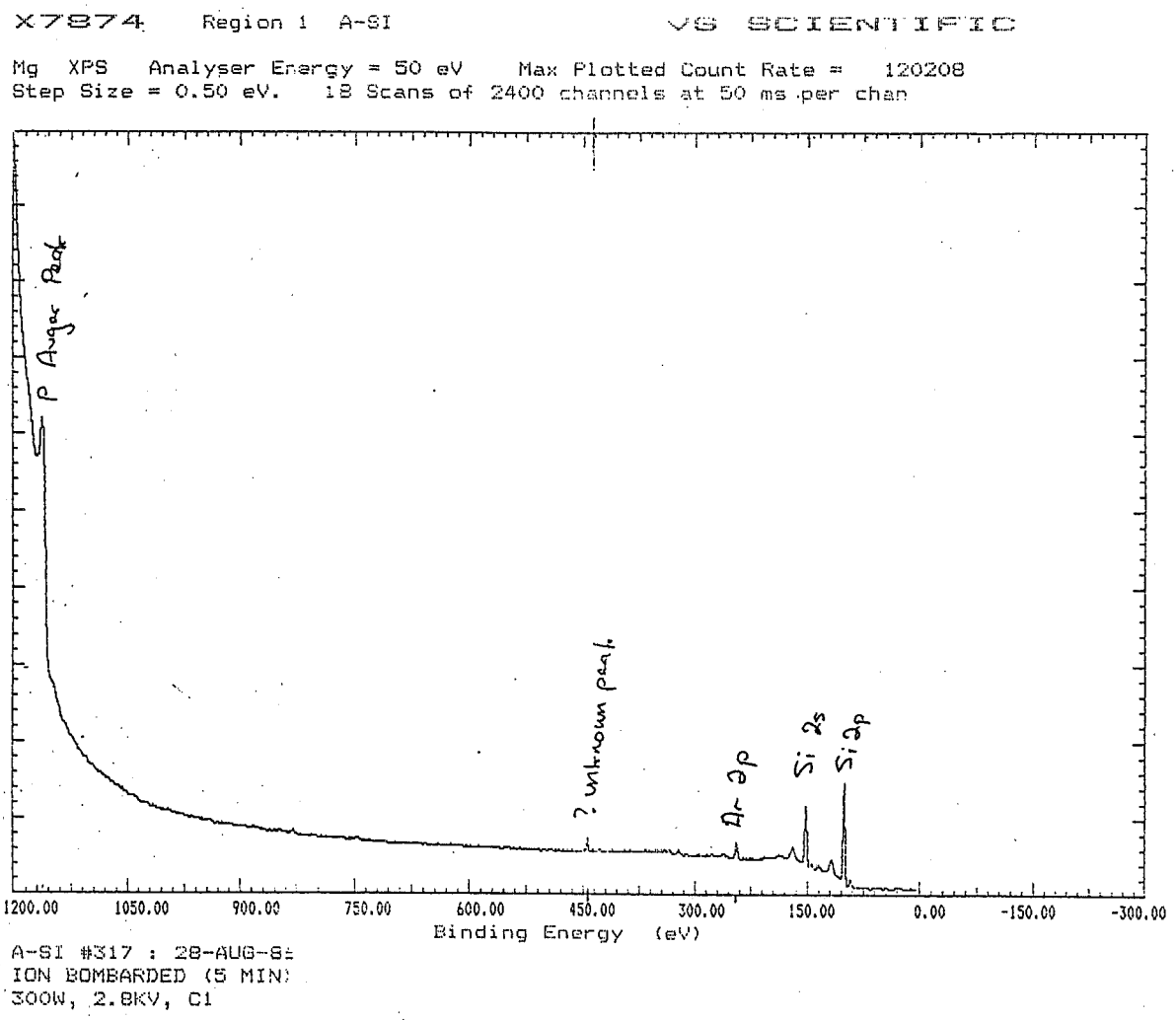
X7874 Region 1 A-SI
VG SCIENTIFIC
Mg XPS Analyser Energy = 50 eV Max Plotted Count Rate = 120208
Step Size = 0.50 eV. 18 Scans of 2400 channels at 50 ms per chan
O Auger Peak
? unknown peak
Ar 2p
Si 2s
Si 2p
1200.00
1050.00
900.00
750.00
600.00
450.00
300.00
150.00
0.00
-150.00
-300.00
Binding Energy (eV)
A-SI #317 : 28-AUG-8
ION BOMBARDED (5 MIN)
300W, 2.8KV, C1

FIGURE 4.18

(2) The oxygen was only a surface oxide layer, not more than 100 Å thick, and was not incorporated in the bulk. As can be seen in Fig. 4.18, the oxygen peaks (both oxygen KLL Auger and 01s,532 eV peaks) have disappeared. This suggests that within the limits of detection there is no oxygen contamination in the bulk. Further investigation of other samples is being carried out to confirm this.

(3) Several peaks need further investigation as they are not recognisable as known XPS peaks. An Aℓ Kα survey is needed to show whether they are Auger peaks or not.

(4) Ion bombardment of both doped samples enabled a positive identification of phosphorus (peak between 100 and 115 eV [Kinetic energy]) on both #353 and #317 (Fig. 4.19). Due to the nature of Argon ion bombardment (e.g. different sputtering rates between elements and concentration effects) the peak is of dubious quantitative value (even with the use of standards). However, it can still be used for qualitative work.

4.4. Substrate Effects Investigated by XPS

To investigate the composition of the a-Si:H films and their interaction with the substrate, an XPS depth profile was performed by Chris Lund and Craig Klauber at C.S.I.R.O., Bentley on thin (≈0.1 μm) a-Si films on both 304 and 316 stainless steel substrates, as described in Section 3.2.3, at 300W and 2.8 kV.

As can be seen from Figs. 4.20 and 4.21, an insulating oxide layer occurs at both surfaces of the a-Si:H film. There is a thin (≈130 Å) oxide layer on the surface exposed to air and a second much thicker (≈700 Å) oxide layer between the a-Si:H film and the stainless steel substrate, due to the passivation of the substrate. Between these two layers in both samples is a layer of intrinsic a-Si:H. At a depth of about 420 Å the underlying substrate becomes visible - firstly the Fe and then the Cr in the 304 SS, and in the case of the 316 SS, the Fe and Cr together. Nickel appears at a depth of about 720 Å in both with the Mo in 316 SS occurring at about the same time. The profile also seems to suggest that the passivating oxide layer continues for a short distance after the a-Si:H layer ends. No other elements are detectable in the film and substrate except for a monolayer of carbon contamination on the surface of the film.

The thicknesses quoted in Figs. 4.20 and 4.21 are based on the thickness of two red fringes visible on the surface of the film. All other measurements are based on a sputtering rate of 20 Å/min., which was derived from the above thickness divided by the time required to sputter until no silicon is visible in the spectrum.

4.5. Hydrogen Content of the Films

Two approaches have been used to confirm the presence of hydrogen in the a-Si:H films that we have produced. Infrared spectroscopy can be used to detect the Si-H vibrational modes. There is ample evidence in the literature of the applicability of this technique. We had available some glow discharge samples produced in Edinburgh and these showed the characteristic spectrum as described by Saraie et al [16]. Early attempts to detect Si-H bands in our CVD films encountered difficulties due to the strong interference fringes masking the Si-H signals. To

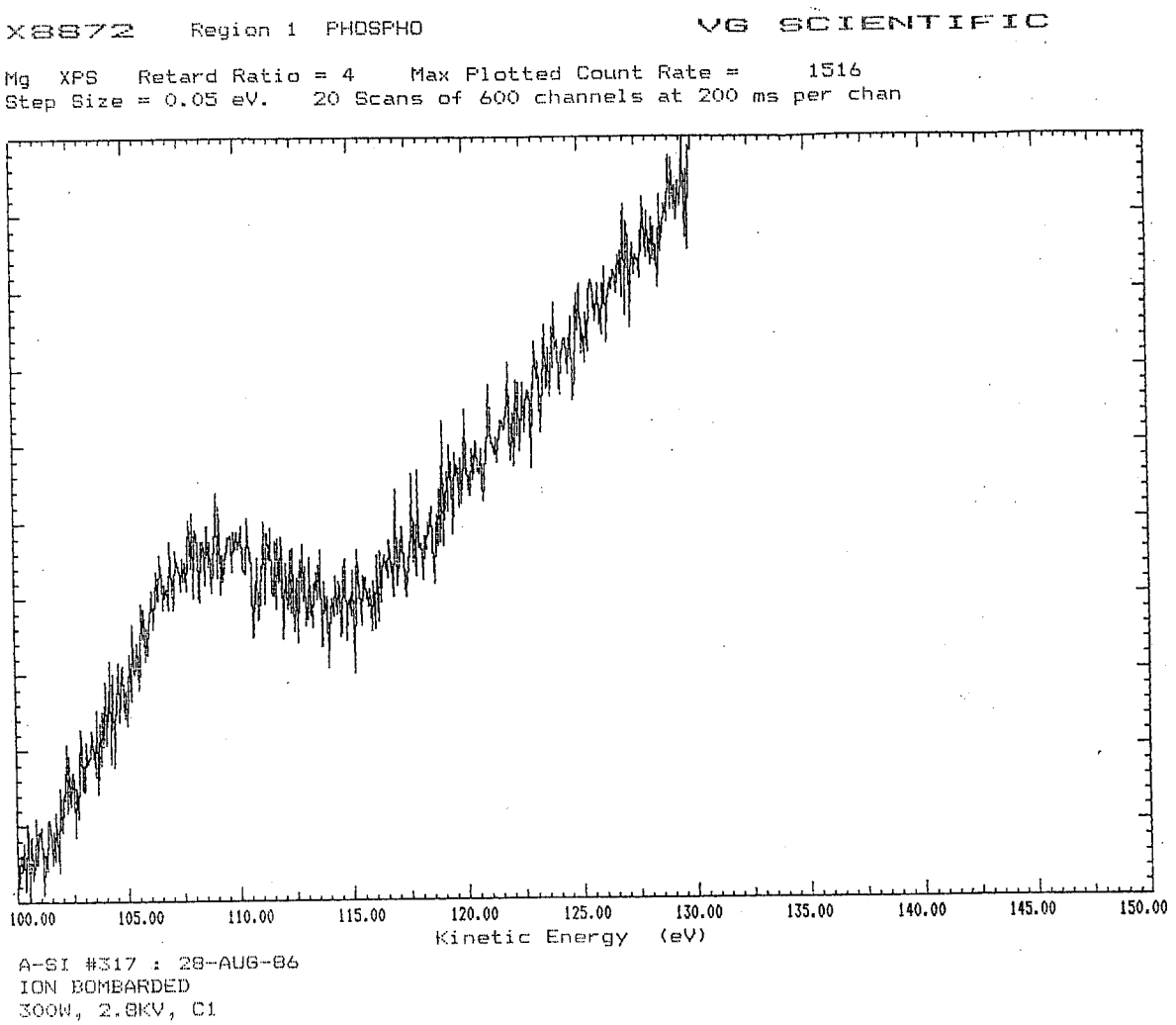
X8872 Region 1 PHOSPHO
VG SCIENTIFIC
Mg XPS Retard Ratio = 4 Max Plotted Count Rate = 1516
Step Size = 0.05 eV. 20 Scans of 600 channels at 200 ms per chan
100.00
105.00
110.00
115.00
120.00
125.00
130.00
135.00
140.00
145.00
150.00
Kinetic Energy (eV)
A-SI #317 : 28-AUG-86
ION BOMBARDED
300W, 2.8KV, C1

FIGURE 4.19

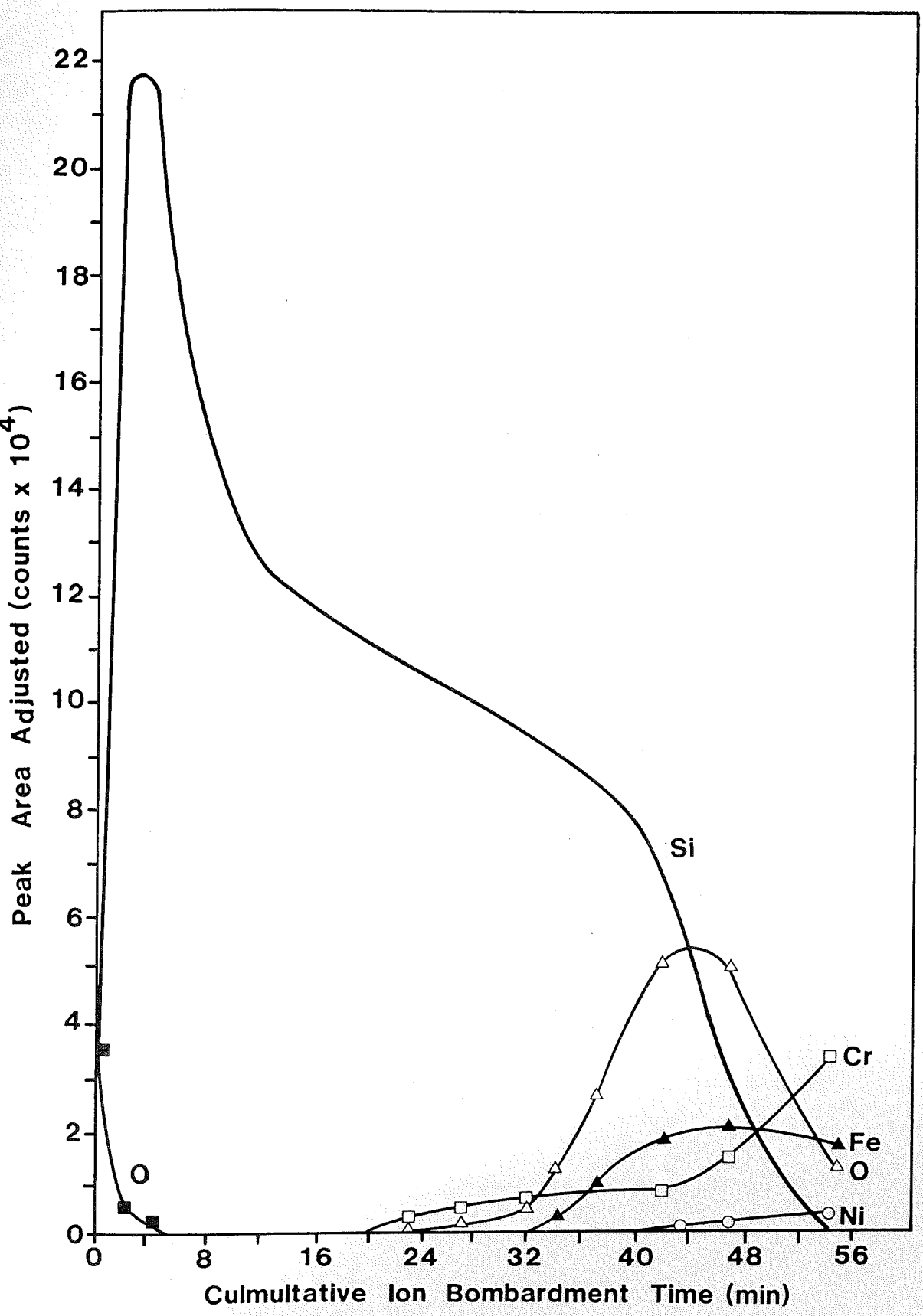

FIGURE 4.20 Auger depth profile of thin film a-Si:H on 304 stainless steel with standard passivation.

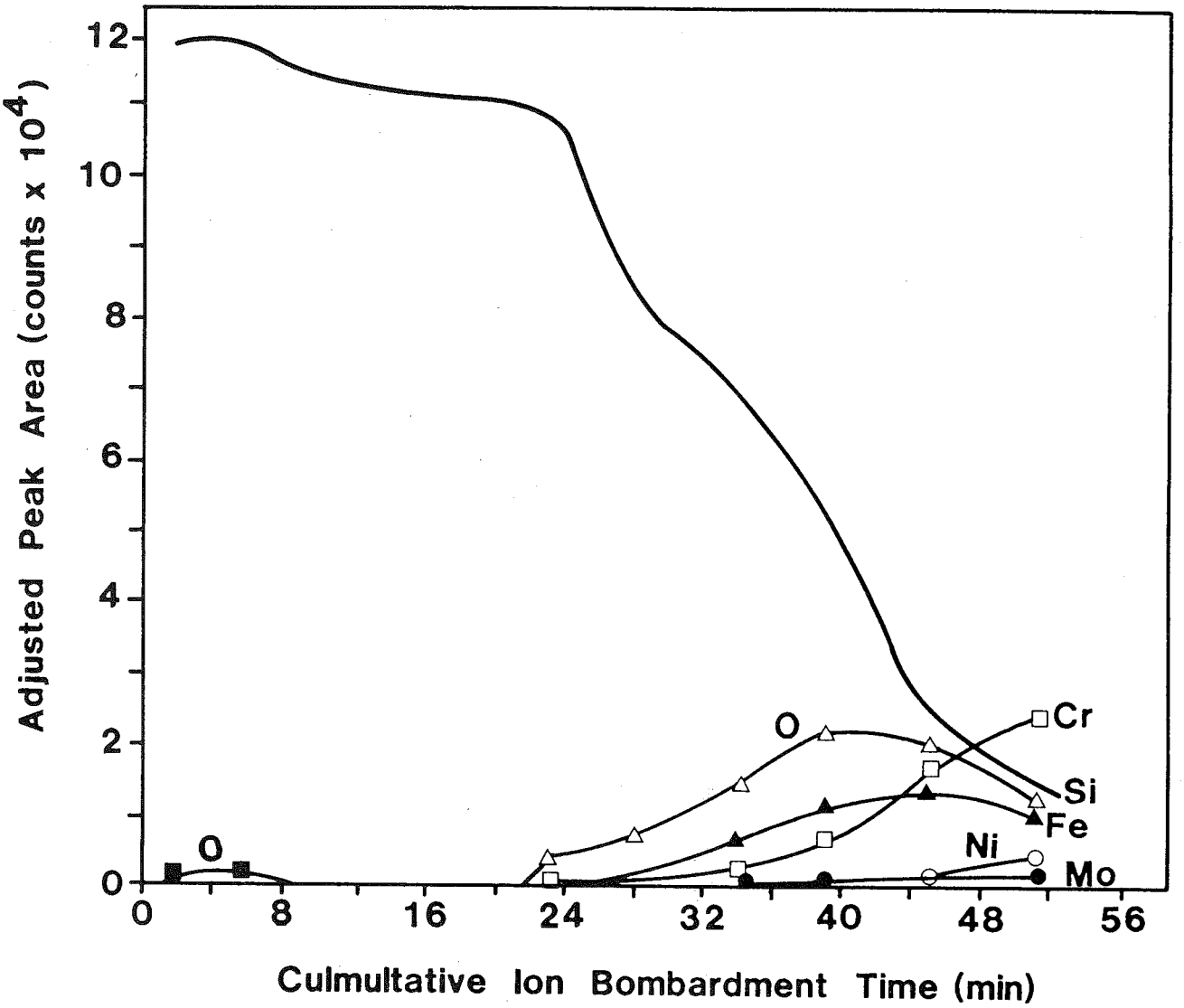

FIGURE 4.21 Auger depth profile of thin film a-Si:H on 316 stainless steel with standard passivation.

overcome this, samples were prepared on roughened crystalline silicon and a transmission spectrum obtained (Fig. 4.22). The spectrum showed a strong Si-H stretching mode near 2000 wavenumbers. Integration of this peak gave a hydrogen content of 2 atomic percent.

The similarity of the films produced on different substrates leads us to believe that the films on stainless steel will have a similar hydrogen content. To confirm this, a second technique of thermal desorption has been used (Cai et al, Morimoto et al [17,18]). On heating the substrate in vacuum, hydrogen evolution may be measured using a mass spectrometer. The thermal desorption spectrum (Fig. 4.23) shows two peaks, one at ~360°C, the other at ~560°C. We are currently investigating the role of each one and the bonding structure they represent. Morimoto et al [18] have shown that the desorption temperatures change with the incorporation of N in the a-Si. It is possible that the temperatures may be useful as a measure of impurity content.

The low atomic percentage of H found in these CVD films is probably due to the high temperature (~450°C) at which they were deposited. Other authors [19] have shown that thermal CVD material has less of the weakly bound H which desorbs at 350°C because the deposition temperatures generally exceed this threshold. An aim of future CVD work must therefore be to find ways of reducing the deposition temperature to below 350°C. Also, the role of this weakly bound H in the a-Si:H lattice must be carefully studied.

4.6. Conductivity

The dark conductivity of a-Si:H samples has been determined as a function of temperature by measuring their voltage drop and current across metal contacts deposited on the samples. Terms used and a diagram of the arrangement is shown in Fig. 4.24.

The aluminium contacts were vacuum-evaporated through a mask on to the films. The thickness of the silicon films was previously determined by a surfometer measurement, while the width and length between the two metal contacts are defined by the mask.

The samples were preannealed at 250°C for 20 minutes in forming gas (20% H_2, 80% N_2) before any measurement was made. Under measurement, a DC potential of 30 V is applied across the metal contacts and the current is measured by a picoammeter. The sample is enclosed in an aluminium diecast box to minimize electrical interference (since the current measurement is in the order of nanoamperes). The temperature of the sample is monitored by a K-type thermocouple placed beneath the sample.

The sample is immersed in liquid nitrogen and then removed and allowed to warm up to ambient temperatures. Measurements of voltage, current and temperature are monitored as the sample warms up.

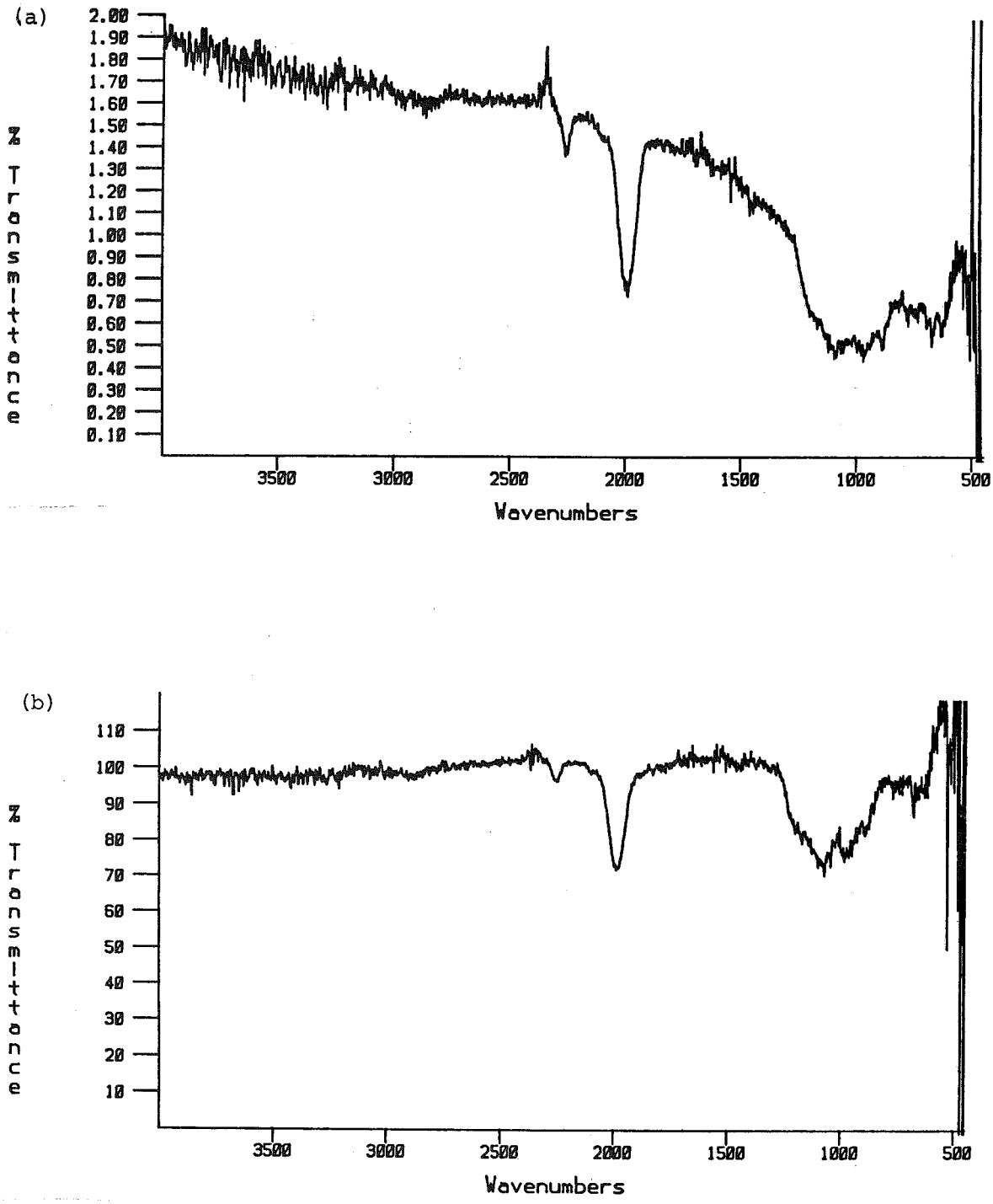

FIGURE 4.22 IR vibrational spectra for sample S104 :
(a) expanded spectrum, as obtained;
(b) spectrum after normalisation to 100% maximum transmission.

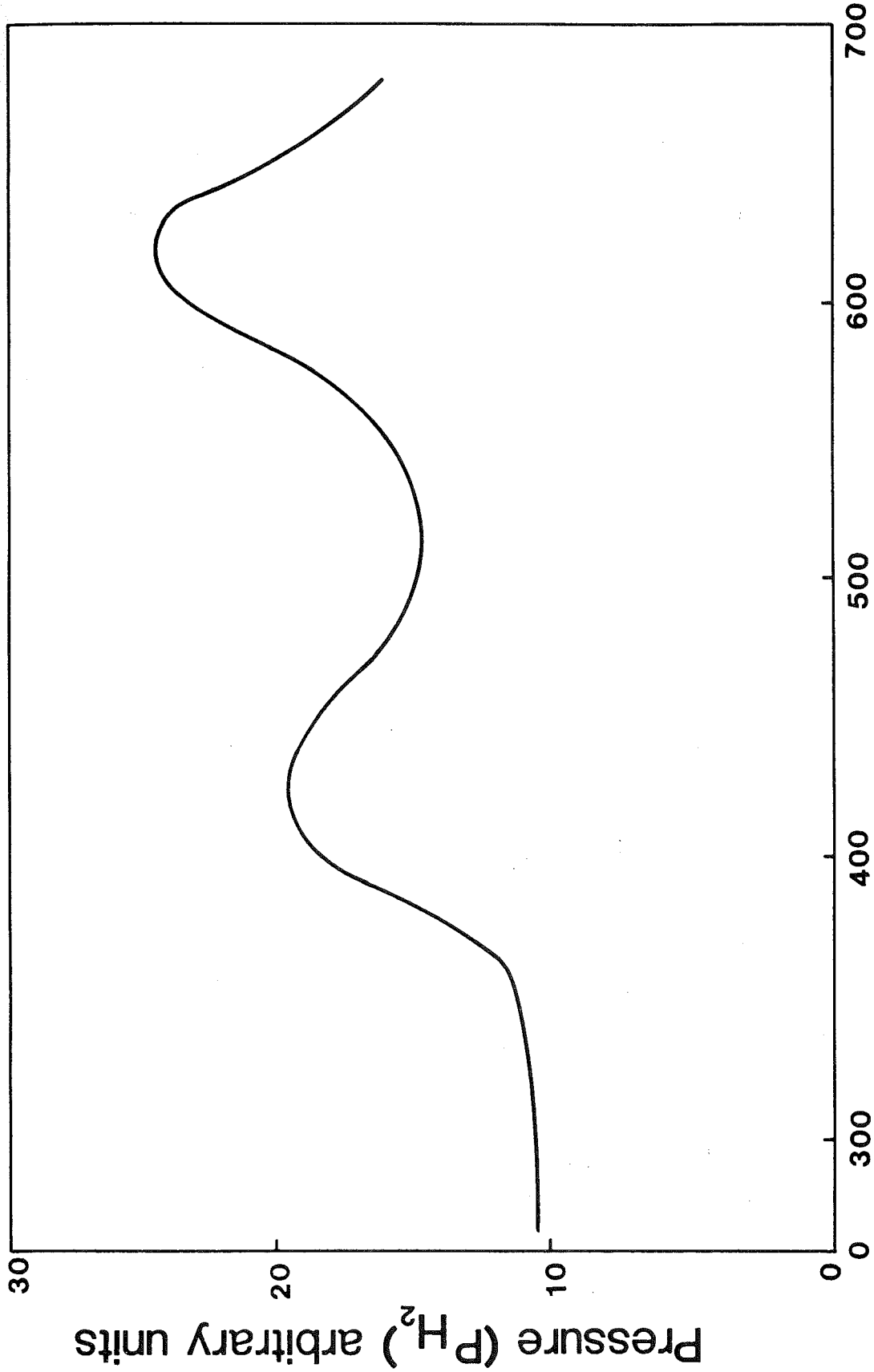

FIGURE 4.23 Thermal desorption of H_2 from a-Si:H film.

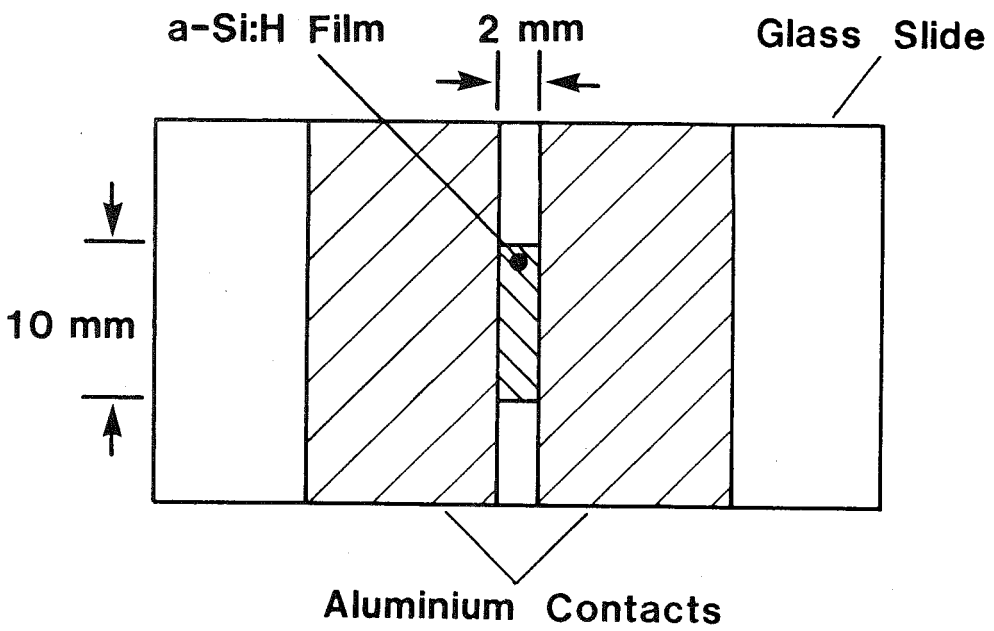

FIGURE 4.24 Sample prepared for resistivity measurement.

5. FABRICATION OF SOLAR CELL STRUCTURES FROM a-Si

Owing to the nature of the hydrogen incorporation in the amorphous silicon and its low bonding energy, all processing carried out on the films must be done at low temperatures (below 300°C). Work therefore has been on Schottky barrier or metal-semiconductor devices, which are simple to fabricate and which can be done without subjecting the film to a high temperature furnace stage, although care has to be taken with radiated heat during the metal evaporation procedures.

Saturation of the dangling silicon bonds in the films with hydrogen causes the material to be electronically n-type so that a choice of metal must be made from materials with high work functions to induce the required p-inversion layer. Platinum has the highest work function of the metals and has been used in this work.

5.1. Processing

The devices are found to show marked gains if the films are first annealed in a furnace at 250°C for 20 minutes in a stream of forming gas. Improvements of about 20% are typical.

For metallization, small pieces of Pt wire of 99.99% purity are initially etched in acid to remove surface contaminants and are loaded into a molybdenum or tungsten boat in a high vacuum system. The stainless steel substrates, on which the films are deposited, are then placed on masks above the boats and the system is pumped down to $\sim 10^{-6}$ torr.

A number of procedures are used with different masks to permit various areas of the surface to be covered with platinum. If surface defects are present, giving a low shunt resistance, then covering the whole area will cause a short and give a zero result. It is therefore prudent to cover the films with a large number of small squares or circles. If all are active, then the film can be assumed to be uniform and good devices should result from such thin film growth procedures.

The metal is evaporated into the substrates, forming a transparent film approximately 300 ~ 500 angstroms thick. The system is then brought up to atmospheric pressure and the substrate is placed in a second mask which permits very small dots of contact metal to be deposited on the Schottky films. Silver is usually used for this contact.

Both deposition procedures are carried out rapidly to minimize the amount of heat applied to the films.

The substrates are then allowed to cool slowly and the system is brought up to atmospheric pressure with dry nitrogen and the substrates removed.

Measurements of the optical properties of the devices are made immediately after removal, under a lamp which has an output equivalent to AM1, with both the open circuit voltage and the short circuit current being evaluated.

After measurements, it is usually found beneficial to again anneal the devices at 250°C in a temperature-controlled furnace in a forming gas ambient for 20 minutes. This technique has produced improvements

of about 10% and also produced some recovery properties with cells of low output.

Some of the devices had an anti-reflective coating of tantalum-silicafilm deposited on them by a spin-on technique.

5.2. Results

Good films generally produced open circuit voltages of about 300 mV with a maximum for small area devices of 430 mV. The best large area device (2 cm squared) produced 364 mV and 3.6 μA. The highest, short circuit current density obtained was 0.4 mA/cm^2.

6. CONCLUSIONS

This project has been in progress for nearly two years. Some encouraging results have been obtained :

(a) The open circuit voltages of the Schottky barrier solar cells obtained by this approach are quite encouraging.

(b) The silent electrical discharge technique has produced enhanced deposition rates for the a-Si:H thin films.

(c) XPS analysis has shown that the high resistivity of the films is partly due to thick oxide layers at the front and back surfaces of the films. There does not appear to be any substantial oxygen contamination of the bulk a-Si:H material.

(d) The CVD process is simple and very safe and appears to give reasonably good semiconducting material. Using a variety of chemical and physical techniques we have begun to characterise these a-Si:H films and identified several problems which need to be overcome if the performance of the photovoltaic devices are to be improved.

The main problems at present are :

(e) The resistivity of the films is high due to the presence of thick oxide layers on the front and back surfaces of the films. We are attempting to eliminate this problem by developing new passivation techniques and by preparing devices in situ.

(f) The thickness of the a-Si:H films has not been optimized for maximum performance.

(g) The use of an anti-reflection coating would give considerable improvements in current densities because the a-Si:H films are highly reflective.

(h) Leaky films have made it difficult to prepare large area devices. We have attempted to improve the cleanliness of our laboratory to reduce these problems.

(i) The use of high deposition temperatures in CVD leads to a shortage of weakly-bonded H in the a-Si:H lattice. This can only be overcome by modifying the gas stream to include substrates which decompose to give a-Si:H at lower temperatures. Experiments with mercury-assisted CVD [10] and hydrofluorinated silanes [20] are planned.

We are also experimenting with preparing Schottky devices by depositing a-Si:H on metal films on glass substrates to overcome the problem.

There are also several other obvious improvements which are planned for the forthcoming year. These include :

(1) The optimisation of the deposition temperatures to improve the deposition rate of the a-Si:H films.

(2) The doping of the films and the preparation of *pin* devices in situ.

(3) The development of improved substrate passivation techniques to reduce oxide barriers at the back contact.

(4) The use of hydrofluorinated silanes in the gas stream. These are reported to have a beneficial effect on the stability and conductivity of the films. They also decompose to form a-Si:H,F at lower temperatures.

Further characterisation of the films is also planned with the aim of understanding the electronic structure of a-Si:H and the role played by H and F in the lattice. Further fundamental work is also planned on the nature of the substrate amorphous silicon interaction with a view to optimizing the properties of the substrate.

6. REFERENCES

[1] R.C. Chittick, J.H. Alexander and H.F. Stirling, J. Electrochem. Soc. 116 (1969) 77.

[2] W.E. Spear and P.G. Le Comber, Solid State Communications 17 (1975) 1193.

[3] D. Adler and H.M. Kizilyalli, Alternative Energy Sources 4 (3) (1982) 103.

[4] A. Madan, Topics in Applied Physics 55 (1984) 245.

[5] J. Stuke, Annual Reviews of Materials Science 15 (1985) 79.

[6] F.B. Ellis and R.G. Gordon, J. Appl. Phys. 54 (1983) 5381.

[7] S.R. Kurtz, J. Proscia and R.G. Gordon, J. Appl. Phys. 59 (1986) 249.

[8] F.B. Ellis, R.G. Gordon, W. Paul and B.G. Yacobi, J. Appl. Phys. 55 (1984) 4309.

[9] E.J. Spanier and A.G. MacDiarmid, Inorganic Chemistry 1 (1962) 432.
S.D. Gokhale, J.E. Drake and W.C. Jolly, J. Inorg. Nucl. Chem. 27 (1965) 1911.

[10] N. Matsukura, Y. Katoh and Y. Machi, J. Appl. Phys. 60 (1986) 3364.

[11] S.S. Hegedus, R.E. Rocheleau, J.M. Cebulka and B.N. Baron, J. Appl. Phys. 60 (1986) 1046.

[12] F.B. Ellis Jr, Ph.D. Thesis, Harvard University (1983).

[13] I. Sakata and Y. Hayachi, Jpn J. Appl. Phys. 20 (1981), 675.

[14] A.M. Goodman, Applied Optics 17 (1978) 2779.

[15] J. Tauc, R. Grigorovici and A. Vancu, Phys. Stat. Solidii 15 (1966) 627.

[16] J. Saraie, Y. Fujh, M. Yoshimoto, K. Yamazoe and H. Matsunami, Thin Solid Films 117 (1984) 59.

[17] Z-T Cai, H.E. Ke-lun, Z-A Li and R-G Cheng, Solar Energy Materials 12 (1985) 43.

[18] A. Morimoto, I. Kobayashi, M. Kumeda and T. Shimiza, Jpn J. Appl. Phys. 25 (1986) L752.

[19] A.E. Delahoy, SERI Report STR-211-2637 (1984).

[20] H. Matsumura and H. Tachibana, Appl. Phys. Lett. 47 (1985) 833.